Emission characteristics of black carbon in anthropogenic and biomass burning plumes over California during ARCTAS-CARB 2008

L. K. Sahu,[1] Y. Kondo,[2] N. Moteki,[2] N. Takegawa,[3] Y. Zhao,[4] M. J. Cubison,[5,6] J. L. Jimenez,[5] S. Vay,[7] G. S. Diskin,[7] A. Wisthaler,[8] T. Mikoviny,[8] L. G. Huey,[9] A. J. Weinheimer,[10] and D. J. Knapp[10]

Received 30 December 2011; revised 28 June 2012; accepted 3 July 2012; published 17 August 2012.

[1] The impact of aerosols on regional air quality and climate necessitates improved understanding of their emission and microphysical properties. The size distributions of black carbon (BC) and light scattering particles (LSP) were measured with a single particle soot photometer on board the NASA DC-8 aircraft during the ARCTAS mission 2008. Air sampling was made in the air plumes of both urban and forest fire emissions over California during the CARB (California Air Resources Board) phase of the mission. A total of eleven plumes were identified using SO_2 and CH_3CN tracers for fossil fuel (FF) combustion and biomass burning (BB), respectively. The enhancements of BC and LSP in BB plumes were significantly higher compared to those in FF plumes. The average mass concentration of BC in BB plumes was more than twice that in FF plumes. Except for the BC/CO ratio, distinct emission ratios of BC/CO_2, BC/CH_3CN, CH_3CN/CO, and CO/CO_2 were observed in the plumes from the two sources. Similarly, the microphysical properties of BC and LSP also showed distinct behaviors. The BC count median diameter (CMD) of 115 ± 5 nm in FF plumes was smaller compared to 141 ± 9 nm in the BB plumes. BC aerosols were thickly coated in BB plumes, the average shell/core ratios were 1.47 and 1.24 in BB and FF plumes, respectively. In the total mass of submicron aerosols, organic aerosols constituted about 67% in the FF plumes and 84% in BB plumes. The contribution of sulfate was also significant in the FF plumes.

Citation: Sahu, L. K., et al. (2012), Emission characteristics of black carbon in anthropogenic and biomass burning plumes over California during ARCTAS-CARB 2008, *J. Geophys. Res.*, *117*, D16302, doi:10.1029/2011JD017401.

1. Introduction

[2] Aerosols play an important role in the earth's climate system due to both direct and indirect radiative effects [*Intergovernmental Panel on Climate Change* (*IPCC*), 2007]. The variability in the distributions of aerosols, their chemical speciation, and aerosol-cloud-radiation interactions constitute the largest source of uncertainty in climate models [*IPCC*, 2001; *Conant et al.*, 2002]. Black carbon (BC) is one of the most important atmospheric aerosols and exerts a positive radiative forcing by absorbing solar radiation and a negative forcing by acting as cloud condensation nuclei (CCN) [*Conant et al.*, 2002; *Nenes et al.*, 2002]. However, heating by BC aerosols can cause evaporation of cloud droplets semi-directly, and hence a reduction of the cloud albedo results in a warming of the surface [*Hansen et al.*, 1997; *Ackerman et al.*, 2000]. The contributions of BC aerosols to the radiative forcing on both regional and global scales are significant [*IPCC*, 2007; *Ramanathan et al.*, 2007]. In the free troposphere, elevated layers of BC have large impacts on regional climate and the hydrological cycle through local heating [*Ramanathan et al.*, 2001; *Menon et al.*, 2002]. In polluted regions, high concentrations of BC can have adverse impacts on human health [*Lighty et al.*, 2000; *Nel*, 2005] and atmospheric visibility [*McMeeking et al.*, 2005].

[1]Physical Research Laboratory, Ahmedabad, India.
[2]Department of Earth and Planetary Science, Graduate School of Science, University of Tokyo, Tokyo, Japan.
[3]Research Center for Advanced Science and Technology, University of Tokyo, Tokyo, Japan.
[4]Air Quality Research Center, University of California, Davis, California, USA.
[5]Department of Chemistry and Biochemistry and CIRES, University of Colorado Boulder, Boulder, Colorado, USA.
[6]Now at Tofwerk AG, Thun, Switzerland.
[7]NASA Langley Research Center, Hampton, Virginia, USA.
[8]Institute of Ion Physics and Applied Physics, University of Innsbruck, Innsbruck, Austria.
[9]School of Earth and Atmospheric Sciences, Georgia Institute of Technology, Atlanta, Georgia, USA.
[10]Atmospheric Chemistry Division, National Center for Atmospheric Research, Boulder, Colorado, USA.

Corresponding author: L. K. Sahu, Physical Research Laboratory, Navarangpura, Ahmedabad 380009, India. (lokesh@prl.res.in)

[3] Emissions from incomplete combustion of fossil fuels (FF) and biofuels and biomass burning (BB) are the major sources of BC in the atmosphere [*Penner et al.*, 1993; *Cooke and Wilson*, 1996; *Liousse et al.*, 1996; *Chen et al.*, 2001]. The source sectors of BC include transportation, heating, power generation, industrial processes, biofuel combustion, and BB [e.g., *Streets et al.*, 2003; *Bond et al.*, 2004]. In the global inventory of BC, the emissions from FF, biofuel, and open BB contribute ~38%, 20%, and 42%, respectively [*Bond et al.*, 2004]. Although the contribution of BB is significant, emission estimates of BC are highly uncertain due to the variability in parameters such as the combustion factor, burned area, biomass material.

[4] Measurements of the mass concentration, size distribution, and microphysical properties of BC are still limited and pose challenges in models for the reliable estimation of radiative forcing [*Penner et al.*, 1998; *Lesins et al.*, 2002; *Sandvik et al.*, 2007; *Bauer et al.*, 2010]. In situ measurements of aerosol size distributions are particularly more limited than those of mass concentrations. The relationships between the concentrations of BC and other co-emitted species can be used to identify sources and also to estimate the budget of BC [*Hansen et al.*, 1989].

[5] In the atmosphere, about 90% of BC is found in the fine mode ($PM_{2.5}$, particles up to 2.5 μm in aerodynamic diameter) [*Sahu et al.*, 2011]. Typically, BC mass size distributions exhibit a predominant mode in the size range of 100–1000 nm [*Berner et al.*, 1996; *Shiraiwa et al.*, 2008; *Kondo et al.*, 2011a, 2011b]. Freshly emitted BC particles are initially hydrophobic and externally mixed with non-refractory species and gradually internally mix through condensation and coagulation in the atmosphere [*Jacobson*, 2010]. Eventually BC particles can become hydrophilic due to coating with a sufficient amount of secondary compounds (organic and inorganic) and act as CCN in the atmosphere. Internally mixed BC particles can be more hygroscopic and easily removed by wet scavenging compared to externally mixed BC [*Zuberi et al.*, 2005; *Petters et al.*, 2009]. *Moteki and Kondo* [2007] have studied the evolution of the BC mixing state in the laboratory using the single particle soot photometer (SP2) system. Field measurements of the mixing state of individual BC particles are still limited [e.g., *Schwarz et al.*, 2008; *Shiraiwa et al.*, 2008; *Subramanian et al.*, 2010]. *Akagi et al.* [2012] have presented the rate of the transition between externally and internally mixed BC particles emitted by a chaparral fire in California. In urban polluted air, BC becomes internally mixed on a typical time scale of about 12 h due to coating with sulfate (SO_4^{2-}) and organic aerosols (OA) [*Moteki and Kondo*, 2007; *Shiraiwa et al.*, 2008]. On the other hand, coatings develop more quickly in BB plumes than those in previous studies [e. g., *Akagi et al.*, 2012, and references therein]. However, there is no general agreement on soot aging time scales. For example, *Moffet and Prather* [2009] have reported an aging timescale of 3 h in Mexico City using an aerosol time-of-flight mass spectrometer (ATOFMS). Aerosol-radiation interaction depends strongly on the mixing state of aerosols, but the micro-scale mixing of BC is too poorly parameterized in models to determine the climate effects of BC [*Jacobson*, 2000]. The absorption efficiency of BC could be enhanced by factors of 1.5–2.0 if BC is thickly coated with non-refractory compounds [*Bond et al.*, 2006; *Mikhailov et al.*, 2006]. BC aerosols in urban regions tend to be smaller in size and coated more thinly compared to those emitted from BB sources [*Schwarz et al.*, 2008] and therefore may have a longer residence time in the atmosphere [*Akagi et al.*, 2012; *Petters et al.*, 2009].

[6] Several field studies have reported the size distributions of BC in both urban and rural regions of the United States (U.S.) [e.g., *Wolff et al.*, 1982; *McMurry and Zhang*, 1989; *Venkataraman and Friedlander*, 1994; *Berner et al.*, 1996; *Schwarz et al.*, 2008]. It is important to note that the size of BC in these studies may refer to the size of internally mixed particles if measured by inertial separation and impaction techniques, whereas it refers to the cores of particles with the SP2 technique. California is a diverse state with many sources of air pollution. In the past two decades the population has increased by 33%, and the urban economy has grown rapidly [*Cox et al.*, 2009]. The major emissions of aerosols and trace gases are due to the use of fossil fuels, especially around the urban areas of San Francisco (SF) and LA counties. Emissions from a number of other urban areas such as Fresno in the Central Valley (CV) region also make significant contributions to the inventories of many pollutants in California [*De Young et al.*, 2005]. Among the several anthropogenic sources, emission from mobile sources is the single largest contributor of various greenhouse gases and aerosols in California. Based on the analysis of data from the Interagency Monitoring of Protected Visual Environments (IMPROVE) sites (both remote and urban) in California, *Bahadur et al.* [2011] have reported a decline in the annual average BC concentration from 0.46 μg m^{-3} in 1989 to 0.24 μg m^{-3} in 2008. The rate of decline in BC concentration agrees well with the decline in total FF-particle emissions. The spikes in the BC trend in IMPROVE data coincide with the wildfire season in California, and the rate of decline in BC was slowest compared to the other seasons. California has significant wildfire activity, generally starting in mid-May, peaking in August, and ending in October [*Pfister et al.*, 2008]. Using spaceborne observations, the transport of smoke plumes from the west to the east coast of the U.S. has been tracked [*Hoff et al.*, 2005]. In recent years, wildfires in the western U.S. have increased mainly due to severe droughts and abundant fuels [*Westerling et al.*, 2006].

[7] Field studies have shown that BC aerosols in FF-dominated plumes were approximately 100% more efficient warming agents than BB-dominated plumes [*Ramana et al.*, 2010, and references therein]. Reliable measurements of BC mass concentration (M_{BC}) are prerequisite to characterize the emission and microphysical properties of BC aerosols [e.g., *Stier et al.*, 2006; *Koch et al.*, 2009]. Thus far, most global measurements of BC have primarily been conducted using filter techniques such as aethalometers and particle soot absorption photometers (PSAP). These instruments do not provide information on microphysical properties and are subject to artifacts [*Kondo et al.*, 2011a]. The artifacts in the filter-based measurements of M_{BC} are mainly due to the interferences by co-emitted non-refractory aerosols [*Reid et al.*, 2005; *Kondo et al.*, 2009, 2011a]. The reliable measurement of M_{BC} using SP2 based on the laser-induced incandescence (LII) method has been reported during several recent studies [e.g., *Moteki and Kondo*, 2007, 2008; *Schwarz et al.*, 2006, 2008; *Kondo et al.*, 2011a].

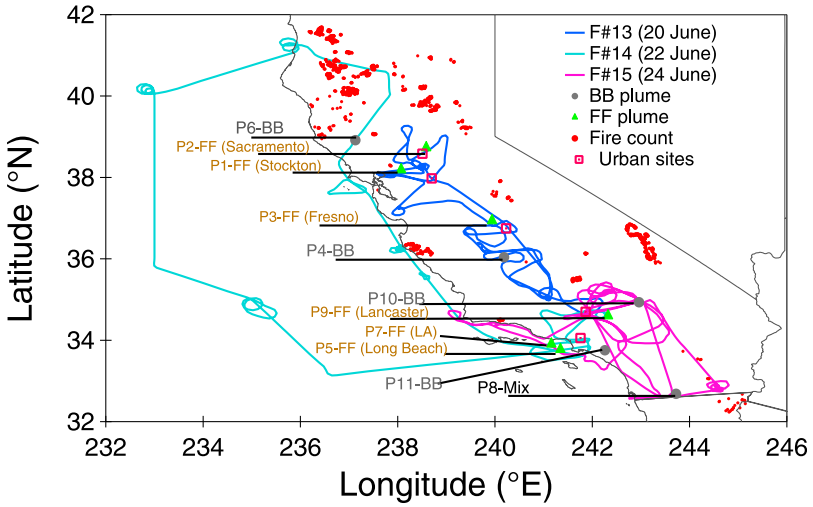

Figure 1. DC-8 flight paths on 20 (F#13), 22 (F#14), and 24 (F#1) June and locations of major plumes over California during the ARCTAS-CARB campaign.

[8] We made measurements of BC and light-scattering particles (LSP) by SP2 on board the NASA DC-8 aircraft over the Arctic, Canada, and California during the Arctic Research of the Composition of the Troposphere from Aircraft and Satellite (ARCTAS) mission in the Spring (ARCTAS-A) and summer (ARCTAS-B) of 2008 [*Jacob et al.*, 2010; *Singh et al.*, 2010; *Kondo et al.*, 2011b; *Matsui et al.*, 2011]. The ARCTAS mission was part of the POLARCAT program during the 2007–2008 International Polar Year (http://www.polarcat.no). As a part of the ARCTAS mission, the California Air Resources Board (CARB) sponsored flights over California and the eastern North Pacific, known as ARCTAS-CARB, in June 2008. The primary objective of the ARCTAS-CARB campaign is to improve the emission inventories of various greenhouse gases, characterize the composition/chemistry of pollutants from shipping and natural sources, and study the impact of the long-range transport of pollutants [*Jacob et al.*, 2010].

[9] The major objective of this work is to characterize the emissions and microphysical properties of BC aerosols emitted from different sources in California. We have focused on the study of air plumes impacted by both FF and BB emissions. Detailed comparisons of aerosol mass concentration, size distribution, mixing state, and emission (or enhancement) ratio between FF and BB plumes are presented here.

2. Aircraft Observations and Data Analysis

2.1. Flight Tracks, Forest Fires, and Meteorology

[10] During the ARCTAS-CARB period the NASA DC-8 aircraft was based in Palmdale, California (34.58 N, 118.1 W) between 17 June and 24 June 2008. The DC-8 performed four flights (a total of ~33 flight hours) on 18 June (ARCTAS flight number, F#12), 20 June (F#13), 22 June (F#14), and 24 June (F#15). The SP2 system had some technical difficulties during the first CARB flight (F#12); therefore, the present study is based on the observations made during the remaining three flights (F#13–15). Figure 1 shows the flight tracks of the DC-8 during ARCTAS-CARB over California. The main objectives of flight F#13 were to study the emissions in urban and rural regions and also to characterize the east-west and north-south gradients of trace gases and aerosols over the CV region. During this flight, a large amount of time was spent sampling the planetary boundary layer (PBL). Flight F#14 was designed to study the coastal regions of California and the evolution of air masses over Long Beach harbor and San Francisco Bay (SFB). An offshore track, with rapid descent into the marine boundary layer (MBL), was planned to provide upwind boundary conditions for regional air quality models. The return leg of flight F#14 included a transect through the northern end of the CV and a low-level transect just off the coast targeting ship emissions. Along the northern coast several wild fire plumes were encountered and visibility was severely impaired. Flight F#15 was the fourth and last sortie of the CARB phase, planned to study the evolution of boundary layer processes and photochemistry over the South Coast Air Basin (SCAB). This flight was also designed to study the transport of pollution from the CV and Mexico. Overall, about 25% of ARCTAS-CARB data collected by the DC-8 was from within the Los Angeles Basin (LAB).

[11] The weather over California was hot and dry during summer 2008, dominated by high pressure centered over the Pacific. The wind flow remained light under cloud-free conditions. Northwesterly winds prevailed over the coastal and CV regions together with sea-land breezes. The predicted mixing layer height (PBLHT) over the ocean was less than 600 m, while over the land it reached up to 1500 m during the daytime [*Huang et al.*, 2011]. Details of the meteorology and impact of large-scale circulation during the campaign period have been reported elsewhere [*Fuelberg et al.*, 2010].

[12] California experienced one of its largest episodes of wild fires, with over 1000 fires burning, in the month of June 2008 [*Singh et al.*, 2010]. Most of the wildfires were located in the mountains of northern California. Emissions from crop residue burning in the CV region can also be significant source of pollutants. On June 21, particularly extensive wildfires were reported at several locations over both northern and southern California. During June 18–20,

Table 1. List of ARCTAS Data Measured Onboard the NASA DC-8 Used in the Present Study

Species	Technique	Accuracy	References
BC mass and number	SP2	±10%	*Moteki and Kondo* [2007, 2010]
LSP number distribution	SP2	±10%	*Moteki and Kondo* [2007, 2010]
LSP volume distribution	SP2	±30%	
Aerosol chemistry	AMS	±35%	*DeCarlo et al.* [2006, 2008] and *Dunlea et al.* [2009]
CO	TDLAS	±2%	*Sachse et al.* [1987]
CO_2	NDIR analyzer	±0.25 ppmv	*Vay et al.* [2011]
CH_3CN	PTR-MS	±10%	*Wisthaler et al.* [2002]
SO_2 (CIT)	CIMS	±50% + 100 pptv	*Crounse et al.* [2006, 2009]
SO_2 (GIT)	CIMS		*Slusher et al.* [2004] and *Kim et al.* [2007]
NOx and NOy	Chemiluminescence	±10% and ±15%	*Weinheimer et al.* [1994]

fires were detected along the California-Mexico border [*Huang et al.*, 2011]. The fire count data (hot spots) detected by the Along Track Scanning Radiometer (ATSR), which represent the locations of major wild fires, are plotted in Figure 1. The detection methodologies used for the ATSR hot spots have been described elsewhere [*Buongiorno et al.*, 1997; *Arino et al.*, 2001].

2.2. Instrumentation

[13] The DC-8 aircraft was equipped with various instruments for the in situ measurement of trace gases and aerosols. *Jacob et al.* [2010] have reported the details of payloads and operational characteristics of these instruments. In addition to the SP2 data, we have used other data sets such as carbon monoxide (CO), carbon dioxide (CO_2), acetonitrile (CH_3CN), methylene dichloride (CH_2Cl_2), sulfur dioxide (SO_2), and submicron aerosol chemical compositions, etc., measured simultaneously onboard the DC-8. The measurement techniques, accuracies, and references for the data used in the present study are summarized in Table 1.

[14] Measurements of the mass size distribution of BC were made using the SP2 system. The detection principle and schematic diagrams of the SP2 have been reported in several papers [*Gao et al.*, 2007; *Moteki and Kondo*, 2007]. Air samples were irradiated with a laser beam at a wavelength of 1064 nm and thus BC particles were heated to incandescence. The peak intensity of the LII signal can be calibrated to obtain the BC mass in the laboratory. The BC particles in ambient air were extracted by removing volatile compounds using a heated inlet to calibrate the SP2 for BC mass. For details of the BC extraction method used in the SP2 system we refer the reader to our previous published works [*Moteki and Kondo*, 2007; *Kondo et al.*, 2011a]. Calibration of the SP2 was routinely performed at the aircraft base during the campaign. Since the detection of BC is based on incandescence, we do not expect any significant change in the calibration parameter depending on the type of plume sampled during the ARCTAS mission. Further details of the calibration method using a differential mobility analyzer (DMA; Model 3081, TSI, Inc. USA)-aerosol particle analyzer (APM; Model-302, KANOMAX, Inc., Japan) system have been given elsewhere [*Moteki and Kondo*, 2007; *Shiraiwa et al.*, 2008]. Detailed descriptions of the calibration of SP2 during ARCTAS period were reported in our recent publications [*Kondo et al.*, 2011a, 2011b]. The mass equivalent diameter of BC (D_{BC}) was calculated by assuming a density of 2.0 g cm^{-3} [*Slowik et al.*, 2004]. The uncertainties due to the dependence of the LII intensity on particle microphysical properties were studied by *Moteki and Kondo* [2010]. The size range of D_{BC} detected by SP2 was 80–860 nm during the campaign. The average fraction of undetected M_{BC} (D_{BC} < 80 nm) was estimated to be 4%. However, the single-mode lognormal fit function of the size distribution was integrated to obtain the total mass concentration of BC (M_{BC}). The overall accuracy in the determination of M_{BC} was estimated to be ∼10%. The diameter of coated BC (shell diameter, D_p) was calculated using the scattering signals of the SP2. The scattering signal data of the SP2 were processed to determine the scattering cross section of LSP. Calibration of the LSP was done using polystyrene latex (PSL) with a refractive index of 1.59 + 0i based on a Mie theory algorithm [*Bohren and Huffman*, 1998]. During this study, LSP with diameters (D_p) in the range of 200–750 nm were detected by the SP2. The average fraction of the undetected volume concentration of LSP (V_{SC}) was estimated to be 18%. The total V_{SC} of LSP was calculated by integrating the lognormal fit functions. We have not adjusted the number concentrations of BC and LSP outside the SP2 detection regions. The fractions of the undetected number concentrations of BC and LSP accounted for less than 15% and 25% of the integrated values, respectively. The uncertainty in deriving V_{SC} was estimated to be ∼30%. In the present study, the values of M_{BC} and V_{SC} are reported in the units of ng m^{-3} and μm^3 cm^{-3}, respectively, at standard temperature and pressure (STP; 273.15 K and 1013.25 hPa). The coating thickness of BC, defined as the shell/core ratio (D_p/D_{BC}), has been used to discuss the internal mixing state of BC.

2.3. Variation of BC Concentration

[15] The time series variations of M_{BC} along with the mixing ratios of SO_2 and CH_3CN using 1-min merged data from three ARCTAS-CARB flights F#13–15 are shown in Figure 2. The M_{BC} varied in the range (5th–95th percentiles) of 7–427 ng m^{-3}, 12–377 ng m^{-3} and 12–725 ng m^{-3} during flights F#13, F#14, and F#15, respectively. During flights F#13 and F#14, the enhancements in M_{BC} were mostly associated with the increase in the levels of either SO_2 or CH_3CN due to the observation of FF or BB plumes, respectively. Mixed plumes (FF + BB) marked by the simultaneous increase in the mixing ratios of both SO_2 and CH_3CN were observed during much of flight F#15. The FF plumes were encountered mostly at lower altitudes close to the surface. On the other hand, the impact of BB plumes was observed at higher levels. On several occasions during flights F#13 and F#15, we did not see any significant

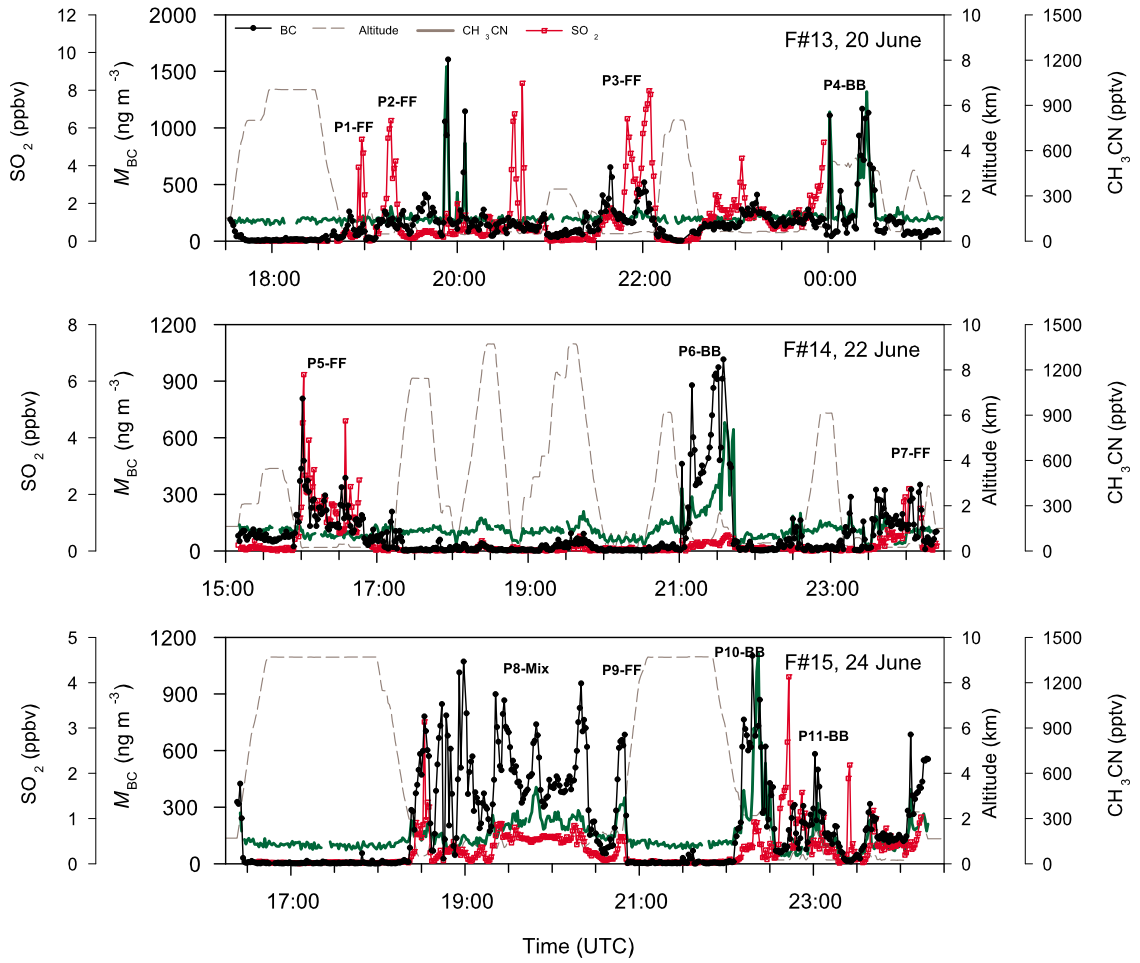

Figure 2. Time series plots of BC mass concentration (M_{BC}), CH_3CN, and SO_2 during three flights, F#13–15, during the ARCTAS-CARB campaign.

changes in M_{BC}, although sharp peaks in SO_2 mixing ratio were noticeable. Based on all the flight data, the enhancements of M_{BC} in BB plumes were significantly larger than those in FF plumes.

[16] Vertical profiles of N_{BC}, M_{BC}, N_{SC}, and V_{SC} and the shell/core ratio are shown in Figure 3. The concentrations of both BC and LSP show large variations due to the observation of plumes originating from different sources and regions of California. Overall, the enhancements in the concentrations of BC and LSP were substantial, as their background concentrations were close to zero for both types of plumes. The aerosol loading was highest in the lower and middle troposphere (below 5 km altitudes), while very few particles were observed in the upper troposphere (5–10 km). The profiles of aerosols varied from flight to flight. The profiles of N_{BC} and M_{BC} exhibited enhanced values within two layers, at 0–1.5 km and 0–5 km, mainly due to the observation of FF and BB plumes, respectively. The vertical profiles of both BC and LSP varied from flight to flight. The concentration of BC aerosols was particularly enhanced during F#13, with a peak M_{BC} of ~1200 ng m^{-3} at ~3.5 km during F#13. The concentrations of BC were relatively low and confined to the lower levels (0–1.5 km of altitudes) over the CV region during flight F#14. The loadings of both BC and LSP were highest and increased with altitude in the lower troposphere over the SCAB region during F#15. The features described for the vertical distributions of aerosols can be subjected to a sampling frequency that varies with altitude and from flight to flight. However, the point we are highlighting is that the impacts of FF and BB plumes were in the approximate ranges of 0–1.5 km and 0–5 km, respectively. Vertical profiles of the shell/core ratio did not show any clear trend and remained stable at ~1.15 during F#13 and F#14. In contrast to the observations during F#13–14, the BC particles were more thickly coated, and the shell/core ratio increased with altitude in the lower troposphere during F#15. The average values of the shell/core ratios were 1.21, 1.19, and 1.44 during F#13, F#14, and F#15, respectively.

3. Results and Discussion

3.1. Classification and Characteristics of Plumes

[17] The mixing ratio of CH_3CN has been widely used as a tracer to identify BB plumes [*de Gouw et al.*, 2003; *Li et al.*, 2000]. On the other hand, the mixing ratios of SO_2 and CH_2Cl_2 have been useful for identifying the plumes predominantly influenced by FF combustion sources [*Chen et al.*, 2001; *Brock et al.*, 2011; *Matsui et al.*, 2011]. Scatterplots of CH_3CN-SO_2 and CH_3CN-CH_2Cl_2 are shown in Figure 4. As expected, the data points in the scatterplots of

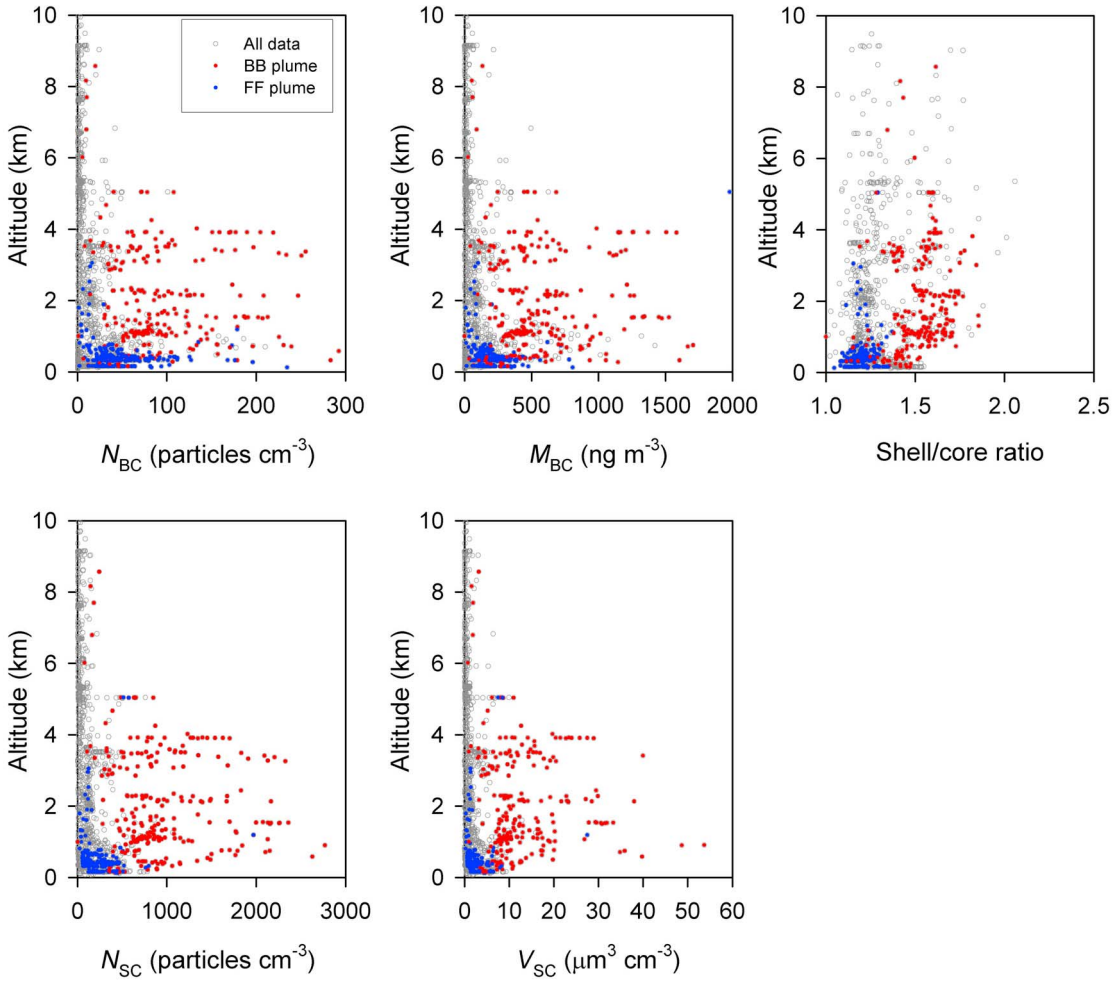

Figure 3. Vertical profiles of BC number concentration (N_{BC}), BC mass concentration (M_{BC}), LSP number concentration (N_{SC}), LSP volume concentration (V_{SC}), and the shell/core ratio during the ARCTAS-CARB campaign.

both CH_3CN-SO_2 and CH_3CN-CH_2Cl_2 populate two distinct groups, one with an elevated mixing ratio of CH_3CN and the other with enhanced values of CH_2Cl_2 and SO_2 due to the measurement of the plumes impacted by BB and FF emissions, respectively. The criteria used to select the plumes vary from study to study depending on the scientific objectives [*Hornbrook et al.*, 2011; *Kondo et al.*, 2011b; *Brock et al.*, 2011]. We have used the following criteria to separate the data for the statistical analysis of the two types of plumes. The threshold for BB plumes was set as data with $\Delta CH_3CN > 300$ pptv, $\Delta CH_2Cl_2 < 50$ pptv, and $\Delta SO_2 < 1500$ pptv. While for the FF plumes, the data points with $\Delta CH_3CN < 250$ pptv, $\Delta CH_2Cl_2 > 50$ pptv, and $\Delta SO_2 > 1500$ pptv were used in the analysis. Moderate concentrations of both these markers were mainly due to the mixing of BB and FF plumes and were designated as mixed plumes (Mix). Moreover, only plumes in which the elevated levels of tracers lasted at least 10 min were considered in the present study. The average ground speeds of the DC-8 aircraft during the sampling of FF and BB plumes were 125 ± 10 m s^{-1} and 141 ± 15 m s^{-1}, corresponding to horizontal distances of 75 ± 6 km and 85 ± 9 km in 10 min, respectively. The tracer criteria have been chosen to minimize the impacts of the mixing of plumes emitted from different sources, as there was always evidence for some urban and agricultural influence in the plumes categorized as BB in California and vice versa [*Yokelson et al.*, 2009; *Hecobian et al.*, 2011]. Since the flight tracks were not designed to chase the evolution of individual plume soon after emission, the exact photochemical status of different plumes is not known.

[18] We have identified 11 major plumes (6 FF, 4 BB, and 1 Mix) over different regions of California during the ARCTAS-CARB period. Three out of four plumes, P1-FF, P2-FF, and P3-FF during F#13 were due to emissions from urban regions of Stockton, Sacramento, and Fresno, respectively, while one BB plume (P4-BB) was observed in the CV region. During F#14, we observed two FF plumes over Long Beach (P5-FF) and LA (P7-FF), with one BB plume (P6-BB) over northern California. During flight F#15, a mixed plume (P8-Mix) was encountered along the Mexico border, along with an urban plume (P9-FF) from Lancaster city and two BB plumes (P10-BB and P11-BB) over the northern part of the SCAB. The approximate locations of these plumes are also shown in Figure 1. The altitude and the average concentrations of M_{BC}, CO, and CH_3CN observed in each of these 11 plumes are given in Table 2. To quantify

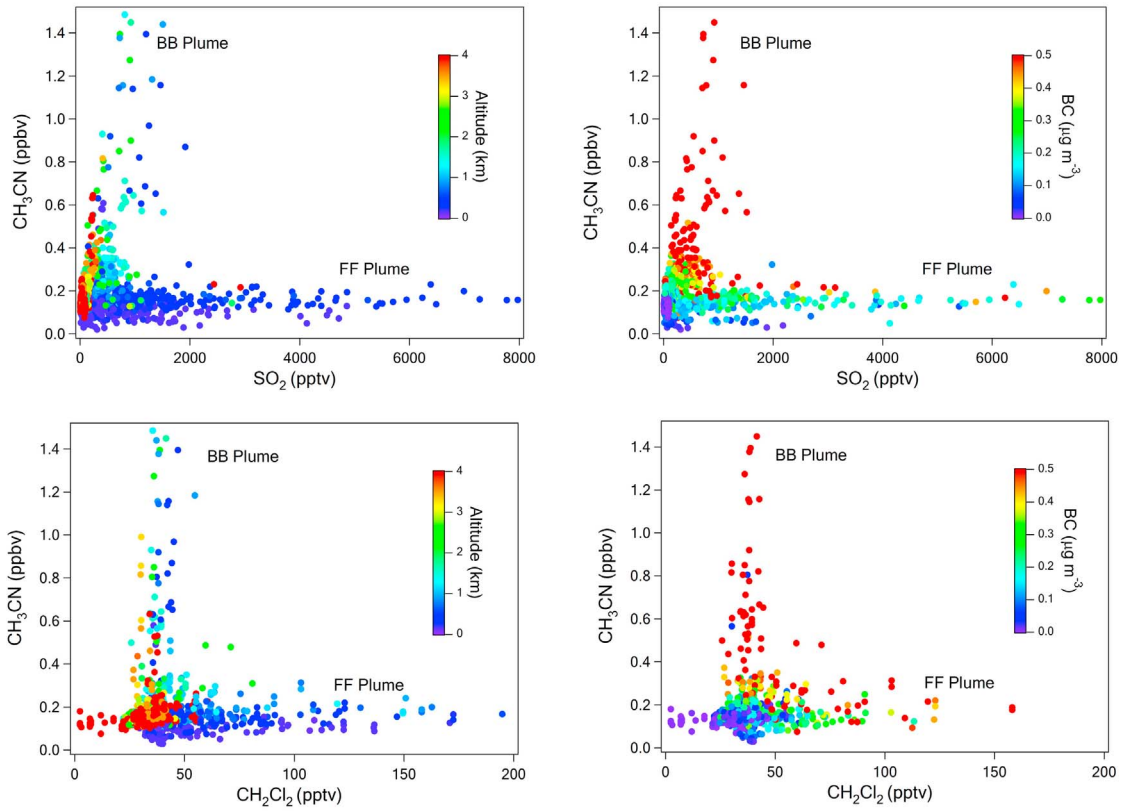

Figure 4. Scatterplots of (top) CH_3CN-SO_2 and (bottom) CH_3CN-CH_2Cl_2 with color-coded (left) altitude and (right) BC mass concentration information.

the emission (enhancement) ratio of aerosols and trace gases in different plumes we first determined their background concentrations. The background concentrations were estimated as the 5th percentiles of the values in every 10-K range of potential temperature (PT) and were interpolated linearly (see Figure 5). The background concentrations of most of the aerosols and short-lived trace gases were close to zero (or near the detection limit) during the campaign, except for CO (80 ± 10 ppbv) and CO_2 (387 ± 0.7 ppmv). The differences (Δ values) between the plume and background concentrations were used to calculate the emission ratios of aerosols and trace gases. Typically, the average values of the BC number concentration (N_{BC}), LSP number concentration (N_{SC}), M_{BC}, CO, and the shell/core ratio in BB plumes were significantly higher than those in FF plumes. However, the comparison is subject to the amount of plume dilution (or aging) that had occurred in each plume. The FF plumes were mostly encountered near the surface (<1500 m of altitudes), while impacts of BB plumes were observed in the lower troposphere up to a height of ~5000 m.

[19] We have used 1-min merged data to classify the plumes, but for the correlation studies we used 10-s data to

Table 2. Characteristics of FF and BB Plumes and Concentrations of Important Species Based on ARCTAS-CARB 2008 Data

Plume Type	Flight	Altitude (m)	BC Num (particles/cc)	M_{BC} (ng m^{-3})	Shell/Core Ratio	CO (ppbv)	CH_3CN (pptv)	MCE
P1-FF	F#13	320–1634	22 ± 19	87 ± 72	1.16 ± 0.08	101 ± 17	142 ± 37	0.997
P2-FF	F#13	319–742	55 ± 27	233 ± 120	1.18 ± 0.05	149 ± 31	149 ± 36	0.993
P3-FF	F#13	328–422	65 ± 29	266 ± 116	1.20 ± 0.03	153 ± 27	159 ± 40	0.995
P4-BB	F#13	3107–3677	122 ± 85	579 ± 393	1.38 ± 0.07	247 ± 124	433 ± 250	0.915
P5-FF	F#14	127–3049	42 ± 36	205 ± 143	1.17 ± 0.06	147 ± 52	113 ± 32	0.995
P6-BB	F#14	763–1713	94 ± 45	676 ± 287	1.46 ± 0.08	521 ± 172	616 ± 219	0.869
P7-FF	F#14	124–2316	31 ± 22	157 ± 95	1.26 ± 0.08	135 ± 43	104 ± 43	0.996
P8-Mix	F#15	256–1592	68 ± 52	500 ± 399	1.31 ± 0.22	161 ± 51	161 ± 67	0.974
P9-FF	F#15	682–1696	101 ± 45	512 ± 170	1.44 ± 0.14	240 ± 33	236 ± 61	0.994
P10-BB	F#15	1094–3008	70 ± 38	454 ± 251	1.66 ± 0.10	217 ± 72	333 ± 128	0.907
P11-BB	F#15	162–2278	42 ± 41	279 ± 290	1.48 ± 0.22	265 ± 216	392 ± 445	0.903
All BB	Mean	1842	90	513	1.47	299	441	0.898
All BB	SD	1033	35	153	0.11	125	106	0.020
All FF	Mean	565	53	243	1.24	154	157	0.995
All FF	SD	283	28	146	0.11	46	62	0.001

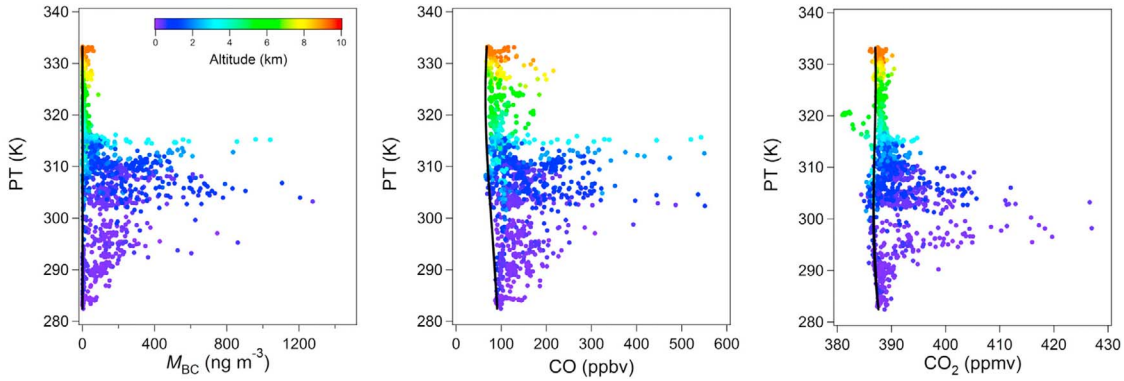

Figure 5. Vertical profiles of BC mass concentration (M_{BC}), CO, and CO_2 over California during ARCTAS-CARB 2008. Potential temperature (PT) is used as the vertical coordinate. The solid red line in each plot is a polynomial fit calculated for the 5th percentile of data in 10-K bins.

get a sufficient dynamic range for the regression analysis. The classification of plume type remained unchanged if the aircraft passed through background air or entered into different plumes for only a brief amount of time. This was done because of the different sampling intervals and response times of the various instruments and also to avoid the complexity in plume identification. In this method of classification, it is possible that some data points may violate the criteria (thresholds) applied for plume selection.

3.2. Estimate of Combustion Efficiency

[20] In the combustion/burning of related sources, the emission factors of aerosols and trace gases depend on the fuel composition (material) and the physical and chemical processes during the emission process. As discussed by *Akagi et al.* [2011], real fires do not usually have distinct phases but are represented by a changing mix of flaming and smoldering processes. The fraction of fuel carbon emitted as particles and trace gases is related to the modified combustion efficiency (MCE). MCE is a useful index of the relative amount of flaming and smoldering combustion that contributed to a smoke sample [*Ward et al.*, 1992; *Akagi et al.*, 2011]. MCE is a simplified form of combustion efficiency (CE). However, the estimate of CE requires the simultaneous measurement of CO_2, incompletely oxidized compounds (CO and NMVOCs), reduced compounds such hydrocarbons (CH_4 and NMHCs), and particulate carbon (PC) [*Ward et al.*, 1991]. The MCE is estimated as the ratio of the amount of carbon emitted as CO_2 to the amount of carbon in the form of CO and CO_2 [*Delmas et al.*, 1995; *Yokelson et al.*, 2008; *Akagi et al.*, 2011].

$$\mathrm{MCE} = \left(1 + \frac{\Delta \mathrm{CO}}{\Delta \mathrm{CO_2}}\right)^{-1} \quad (1)$$

[21] Normally, the difference between CE and MCE is considered to be less than a few percent [e.g., *Guyon et al.*, 2005; *Akagi et al.*, 2011]. In the present study, we have estimated the value of MCE for each plume (Table 2). Average MCEs of 0.898 ± 0.02 and 0.995 ± 0.001 for the BB and FF plumes suggest the predominance of incomplete and efficient combustion, respectively. The distinct values of MCE for FF and BB plumes also confirm that the thresholds used to categorize both types of plumes have been chosen appropriately. The dependence of particle number concentration, mass emission factor, emission ratio, and size distribution on MCE for the forest fires in different ecosystems has been parameterized using both laboratory and field data [e.g., *Janhäll et al.*, 2010; *Akagi et al.*, 2011, 2012]. *Kondo et al.* [2011b] have discussed the dependence of the emission ratios of aerosols on MCE to improve the uncertainty in estimating aerosol emissions from BB sources over the Arctic and Canada. In these studies, the relationships between several aerosol parameters and MCE were investigated.

3.3. Emission Ratio

[22] Emissions data for aerosols and trace gases from different sources are required to assess their impacts on air quality and climate change. In the literature, information about emissions is presented in two basic forms, the emission ratio and emission factor [*Akagi et al.*, 2011, and references therein]. The excess mixing ratio (EMR) of species X is denoted ΔX (X_{plume}-$X_{background}$). The EMR is a highly variable parameter for reactive trace gases and aerosols and depends on post-emission processes. The normalized excess mixing ratio (NEMR = ΔX/ΔY, where Y is a non-reactive smoke tracer) can be measured at the source or for stable species that do not evolve due to photochemistry and mixing. We refer the readers to *Akagi et al.* [2011] for a detailed description of emission-related parameters. The atmospheric evolution of aerosols and trace gases is often characterized by their emission or enhancement ratios [*Andreae and Merlet*, 2001; *Akagi et al.*, 2011]. The emission ratios of various aerosols and trace gases in BB plumes have been extensively studied for fires in the tropical forest ecosystems and savannas [*Janhäll et al.*, 2010; *Akagi et al.*, 2011].

[23] Scatterplots between the enhancements of ΔCO_2, ΔCO, ΔCH_3CN, ΔM_{BC}, and ΔV_{SC} observed in major plumes during all flights are shown in Figure 6. The emission ratios were derived from least square fits constrained to pass through the origin, as the background levels of aerosols and trace gases have already been subtracted. *Kondo et al.* [2011b] have used the averaging method to estimate the emissions during ARCTAS-A and ARCTAS-B. In the

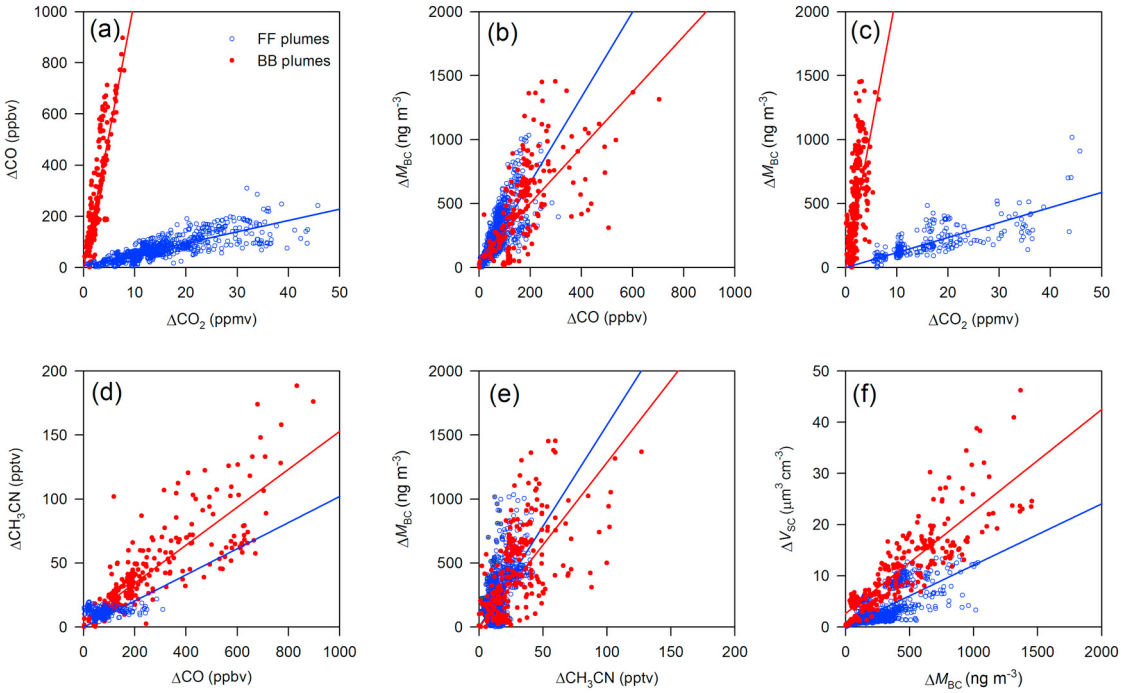

Figure 6. Scatterplots between the enhancements of ΔCO_2, ΔCO, ΔCH_3CN, ΔM_{BC}, and ΔV_{SC} observed in the major plumes during the ARCTAS-CARB campaign.

averaging method, the sum of the enhancement in each data point (ΔX_i and ΔY_i) is used to compute the average emission ratio ($ER_{avg} = \sum_i \Delta X_i / \sum_i \Delta Y_i$). The estimates using these two methods agree well due to the strong correlations in different plumes. The agreement between both these methods was within 10%. The slopes of linear fits have been used to estimate the emission (enhancement) ratios in both BB and FF plumes. The estimated slopes of $\Delta CH_3CN/\Delta CO$, $\Delta CO/\Delta CO_2$, $\Delta V_{SC}/\Delta M_{BC}$, $\Delta M_{BC}/\Delta CO$, $\Delta M_{BC}/\Delta CO_2$, and $\Delta M_{BC}/\Delta CH_3CN$ and respective r^2 values in each plume are given in Table 3. On the other hand, ΔV_{SC} may be affected by photochemical aging; therefore the slope of $\Delta V_{SC}/\Delta M_{BC}$ can be treated as more of an enhancement ratio than just the emission ratio. In the case of poor correlations ($r^2 < 0.4$), the least square fit parameters have not been determined due to large statistical errors.

[24] The atmospheric CO_2 and CO are co-emitted at specific ratios from combustion sources depending on the source and the combustion efficiency [*Wang et al.*, 2010]. Normally the values of $\Delta CO/\Delta CO_2$ are low and fairly stable in plumes impacted by anthropogenic emissions due to the efficient combustion of fossil fuels. On the other hand, the

Table 3. Emission Ratios of BC Mass Concentration (M_{BC}), LSP Volume Concentration (V_{SC}), CO, CO_2, and CH_3CN in Different FF and BB Plumes Over California During ARCTAS-CARB

Plume Type	Flight	CH_3CN/CO (pptv/ppbv)		CO/CO_2 (ppbv/ppmv)		V_{SC}/M_{BC} ($cm^3\ m^{-3}/g\ m^{-3}$)		M_{BC}/CO ($ng\ m^{-3}$/ppbv)		M_{BC}/CO_2 ($ng\ m^{-3}$/ppmv)		M_{BC}/CH_3CN ($ng\ m^{-3}$/pptv)	
		Slope	r^2	Slope	r^2	Slope	r^2	Slope	r^2	Slope	r^2	Slope	r^2
P1-FF	F#13	–	–	3.20	0.67	2.7	0.57	3.65	0.70	14.0	0.70	–	–
P2-FF	F#13	–	–	6.88	0.77	1.9	0.43	2.94	0.60	23.0	0.64	–	–
P3-FF	F#13	–	–	4.96	0.85	9.0	0.56	3.65	0.72	21.0	0.75	–	–
P4-BB	F#13	1.93	0.89	93.0	0.98	17	0.95	4.46	0.80	353	0.79	2.1	0.80
P5-FF	F#14	–	–	4.6	0.66	4.3	0.62	2.3	0.66	10.2	0.60	–	–
P6-BB	F#14	1.12	0.90	151	0.77	18	0.83	3.4	0.73	313	0.82	2.6	0.78
P7-FF	F#14	–	–	4.5	0.63	7.2	0.18	1.9	0.73	8.11	0.62	–	–
P8-Mix	F#15	–	–	26.8	0.81	1.3	0.42	5.4	0.58	159	0.50	–	–
P9-FF	F#15	–	–	6.1	0.84	3.4	0.13	4.5	0.85	31	0.75	–	–
P10-BB	F#15	1.75	0.86	103	0.80	25	0.93	3.15	0.88	268	0.68	1.7	0.77
P11-BB	F#15	2.02	0.86	108	0.97	30	0.92	2.1	0.70	152	0.45	0.92	0.64
All BB	Mean	1.71	0.88	113.75	0.88	23	0.91	3.28	0.78	271.50	0.69	1.83	0.75
All BB	Median	1.84	0.88	105.50	0.89	22	0.93	3.28	0.77	290.50	0.74	1.91	0.78
All BB	SD	0.41	0.02	25.60	0.11	6.0	0.05	0.97	0.08	86.90	0.17	0.75	0.07
All FF	Mean	–	–	5.04	0.74	5.0	0.42	3.16	0.71	17.89	0.68	–	–
All FF	Median	–	–	4.78	0.72	4.0	0.50	3.30	0.71	17.50	0.67	–	–
All FF	SD	–	–	1.30	0.10	3.0	0.21	0.96	0.08	8.69	0.07	–	–

Table 4. Comparison of Emission Ratios of BC Mass Concentration (M_{BC}), CO, and CO_2 With Other BB and FF Plumes

Plume Type	Campaign	CO/CO_2 (ppbv/ppmv)	M_{BC}/CO (ng m^{-3}/ppbv)	M_{BC}/CO_2 (ng m^{-3}/ppmv)
BB	ARCTAS-CARB	113.75 ± 25.6	3.28 ± 0.97	271.5 ± 87
FF	ARCTAS-CARB	5.04 ± 1.3	3.16 ± 0.96	17.9 ± 8.7
BB	ARCTAS-B	80 ± 110	2.3 ± 2.2	180 ± 269
BB	TexAQS	102 ± 25	9.0 ± 2.0	1770 ± 400
FF	TexAQS	9.9 ± 2.7	5.8 ± 1.0	61 ± 13
BB	ARCPAC	42 ± 19	7.0 ± 4.0	NA
FF	Tokyo, Japan	11	5.7	62
FF	Beijing, China	35.6 ± 7.3	4.7 ± 1.2	150 ± 36
BB	Extra tropical Forest (Compiled)	107 ± 38	6.5 ± 3.2	701 ± 245

slopes of $\Delta CO/\Delta CO_2$ are high and exhibit large variability in BB plumes, depending on the phase of fire [*Yokelson et al.*, 2003, and references therein]. In the present study, scatterplots of ΔCO-ΔCO_2 show very good correlations, with average r^2 values of 0.88 and 0.74 in BB and FF plumes, respectively. We find that the data points split into two distinct groups, indicating significant contrast in the ΔCO-ΔCO_2 relations between BB and FF plumes. The average emission ratios of $\Delta CO/\Delta CO_2$ are 5.04 ± 1.3 ppbv $ppmv^{-1}$ and 113.75 ± 25.6 ppbv $ppmv^{-1}$ in FF and BB plume, respectively. As summarized in Table 4, *Schwarz et al.* [2008] have also reported similar ranges of $\Delta CO/\Delta CO_2$ in both BB and FF plumes observed over Houston and Dallas during the Texas Air Quality Study (TexAQS) campaign in 2006. During ARCTAS-B, a slightly lower value of 80 ± 110 suggests the contribution of relatively efficient BB sources and sampling of air masses impacted by different stages of fire over Canada [*Kondo et al.*, 2011b]. The slopes of $\Delta CO/\Delta CO_2$ in BB plumes over California and Canada are within a range of 121 ± 19 ppbv $ppmv^{-1}$ and 67 ± 12 ppbv $ppmv^{-1}$, estimated for smoldering and flaming fires, respectively, in the temperate/boreal ecosystems [*Cofer et al.*, 1991]. The slope of $\Delta CO/\Delta CO_2$ (26.8 ppbv $ppmv^{-1}$) in a mixed plume was between the values estimated for FF and BB plumes. In this study, the value of $\Delta CO/\Delta CO_2$ estimated in each plume has been used to calculate the MCE. As presented in Table 2, the MCE values were estimated to be within the ranges of 0.869–0.915 and 0.994–0.997 in BB and FF plumes, respectively. As expected, the MCE value of the mixed plume was 0.974, and distinct from the ranges estimated for FF and BB plumes.

[25] BC and CO are the co-products of incomplete combustion, and their ratio can be used to estimate the BC emission budget with a prior knowledge of the CO inventory [*Sahu et al.*, 2011]. To assess the impact of long-range transport in remote locations, the ΔM_{BC}-ΔCO relations have also been used to estimate the transport efficiency [*Sahu et al.*, 2009; *Matsui et al.*, 2011]. The emission ratio $\Delta M_{BC}/\Delta CO$ varies greatly between sources [*Miguel et al.*, 1998; *Bond et al.*, 2004]. In this study, the enhancements of ΔM_{BC} and ΔCO show tight correlations in all plumes, with average r^2 values of 0.78 in BB and 0.71 in FF plumes. However, the emission ratios of $\Delta M_{BC}/\Delta CO$ do not show a clear distinction between BB and FF plumes. The estimated values of $\Delta M_{BC}/\Delta CO$ are 3.16 ± 0.96 ng m^{-3} $ppbv^{-1}$ and 3.28 ± 0.97 ng m^{-3} $ppbv^{-1}$ in FF and BB plumes, respectively. These estimates are slightly higher compared to the average value of 2.3 ± 2.2 ng m^{-3} $ppbv^{-1}$ estimated for Canadian BB plumes during ARCTAS-B [*Kondo et al.*, 2011b]. On the other hand, significantly higher slopes of $\Delta M_{BC}/\Delta CO$ of 6.8 ± 1.17 ng m^{-3} $ppbv^{-1}$ and 10.5 ± 2.3 ng m^{-3} $ppbv^{-1}$ were reported for FF and BB plumes, respectively, over Houston and Dallas during TexAQS 2006 [*Spackman et al.*, 2008]. Consistent with the FF emission ratio over the SCAB region, the $\Delta M_{BC}/\Delta CO$ ratio was 2.9 ± 0.9 ng m^{-3} $ppbv^{-1}$ over Mexico during the Megacity Impacts on Regional and Global Environment (MIRAGE) study, part of the larger Megacity Initiative: Local and Global Research Observations (MILAGRO) campaign, based on aircraft measurements [*Crounse et al.*, 2009; *Subramanian et al.*, 2010]. As presented in Table 4, the average emission ratio of $\Delta M_{BC}/\Delta CO$ in BB plumes over California is significantly lower than the values for extra tropical fires [*Andreae and Merlet*, 2001; *Akagi et al.*, 2011]. The ratio $\Delta M_{BC}/\Delta CO$ does not directly depend on the geographic location or observation site; however, it may vary due to several factors prevailing in the region of the observations. *Baumgardner et al.* [2002] have described how the $\Delta M_{BC}/\Delta CO$ ratio varies with the composition of fuel materials, the nature of combustion (e, g., MCE), the proximity of the observation site to the source, and the local meteorological conditions (e. g., clouds and precipitation).

[26] Scatterplots of ΔM_{BC}-ΔCO_2 show good correlations in all the major plumes. However, unlike the ΔM_{BC}-ΔCO relations, the slope of ΔM_{BC}-ΔCO_2 reveals two distinct populations corresponding to FF and BB plumes. The emission ratios of $\Delta M_{BC}/\Delta CO_2$ are 17.9 ± 8.7 ng m^{-3} $ppmv^{-1}$ for FF and 271.5 ± 87 ng m^{-3} $ppmv^{-1}$ for BB plumes. In Canadian BB plumes, the $\Delta M_{BC}/\Delta CO_2$ values were 369 ± 257 ng m^{-3} $ppmv^{-1}$ for smoldering phase and 88 ± 80 ng m^{-3} $ppmv^{-1}$. Exceptionally large enhancement ratios of 2067 ± 467 ng m^{-3} $ppmv^{-1}$ and 71.2 ± 15 ng m^{-3} $ppmv^{-1}$ in BB and FF plumes, respectively, were observed during the TexAQS campaign [*Schwarz et al.*, 2008]. The slope of $\Delta M_{BC}/\Delta CO_2$ in FF plumes over California is significantly lower than the values reported for urban emissions in East Asia (Table 4). As reported in *Akagi et al.* [2012], the $\Delta M_{BC}/\Delta CO_2$ emission ratio of 7.83×10^{-4} mol mol^{-1} estimated downwind of chaparral fire in California was significantly higher compared to the average value of $(2.72 \pm 0.87) \times 10^{-4}$ mol mol^{-1} from BB sources during ARCTAS-CARB.

[27] Emission ratios are highly dependent on the chemical composition of fuel materials. This is especially true for minor compounds; for example, the nitrogen (N) content of burning material may vary with vegetation type and also with the season [*McMeeking et al.*, 2009, and references therein]. Therefore, the emission ratio of CH_3CN can be useful to study the variability in emission ratio across different ecosystems and seasons. Scatterplots of ΔCH_3CN-ΔCO and ΔM_{BC}-ΔCH_3CN show tight correlations ($r^2 > 0.77$) in BB plumes; but, as expected, these were poorly correlated in FF plumes. In the BB plumes, the average slopes of $\Delta CH_3CN/\Delta CO$ and $\Delta M_{BC}/\Delta CH_3CN$ were 1.71 ± 0.41 pptv $ppbv^{-1}$ and 1.83 ± 0.75 ng m^{-3} $pptv^{-1}$, respectively. These emission ratios show reasonable agreement with the values observed in Canadian fire plumes. During the

Aerosol, Radiation, and Cloud Processes affecting Arctic Climate (ARCPAC) campaign, the emission ratios of $\Delta CH_3CN/\Delta CO$ from forest fires and agricultural burning were 2.1 ± 0.8 pptv ppbv^{-1} and 3.1 ± 1 pptv ppbv^{-1}, respectively [*Warneke et al.*, 2009]. *Hornbrook, et al.* [2011] have reported mean observed $\Delta CH_3CN/\Delta CO$ ratios of 1.4 ± 0.4 pptv ppbv^{-1}, 1.4 ± 0.7 pptv ppbv^{-1}, and 1.7 ± 0.4 pptv ppbv^{-1} for Asian, Californian and Canadian BB fires, respectively, using Trace Organic Gas Analyzer (TOGA) data of CH_3CN during the ARCTAS mission. The TOGA analyzer uses fast online gas chromatography coupled with mass spectrometry (GS-MS), analyzing a 40-s integrated sample once every two minutes. The slight differences in $\Delta CH_3CN/\Delta CO$ ratios measured using TOGA and PTR-MS could be due to different sampling and detection methods. Comparison of $\Delta CH_3CN/\Delta CO$ estimated during three different phases of the ARCTAS mission suggests that the ratio does not vary significantly with BB sources. During the Intercontinental Transport and Chemical Transformation experiment in 2002 (ITCT 2K2) [*de Gouw et al.*, 2004, and references therein], the average emission ratio of $\Delta CH_3CN/\Delta CO$ of 1.95 ± 0.11 pptv ppbv^{-1} in Asian plumes over California was much higher compared to 0.1 pptv ppbv^{-1} observed over Los Angeles (FF sources). Our estimates of $\Delta CH_3CN/\Delta CO$ slopes during ARCTAS-CARB fall within the range of 1.2–4.3 pptv ppbv^{-1} compiled for forest fires in different parts of the globe [*Hornbrook et al.*, 2011, and references therein].

[28] The relatively stable $\Delta CH_3CN/\Delta CO$ ratios estimated in the emissions from different BB sources during the three different phases of the ARCTAS mission is consistent with the ranges of emission factors reported in the literature. The emission factors of CH_3CN from tropical forest, extra-tropical forest and agricultural waste fires vary within a narrow range of 0.18–0.19 g kg^{-1} [*Andreae and Merlet*, 2001]. Although the slopes of $\Delta CH_3CN/\Delta CO$ remained fairly stable during ARCTAS, globally $\Delta CH_3CN/\Delta CO$ can have large variations; for example, the emission ratio of CH_3CN emitted from cooking fires can be an order of magnitude higher than those emitted from peat fires [*Akagi et al.*, 2011].

[29] The enhancements in ΔV_{SC} and ΔM_{BC} show tight correlations (with an average r^2 of 0.91) in BB plumes and moderate correlations (average r^2 of 0.42) in FF plumes. The $\Delta V_{SC}/\Delta M_{BC}$ slope of 23 ± 6 cm^3 m^{-3}/g m^{-3} in BB plumes was ~4 times higher compared to those in FF plumes (Table 3). The average values of V_{SC} were 1.8 cm^3 m^{-3} and 12.3 cm^3 m^{-3} in the FF and BB plumes, respectively. In other words, BC particles in BB plumes were associated with a much larger volume of LSP compared to those in FF plumes. Relatively higher volume fractions of LSP in BB plumes could result from thicker coating of BC particles compared to FF plumes. The chemical characteristics of LSP using AMS data are presented in section 5. In agreement with the present estimate for BB plumes, the average $\Delta V_{SC}/\Delta M_{BC}$ was 24 ± 6 cm^3 m^{-3}/g m^{-3} during the ARCTAS-B campaign. LSP was higher in BB plumes because of the predominance of smoldering combustion. Typically, smoldering combustion produces white smoke and flaming combustion produces black smoke [e.g., *Yokelson et al.*, 1997].

[30] The relationship between the emission ratio and MCE can helpful to investigate the dependence on the stage of fire in BB plumes [*Janhäll et al.*, 2010; *Sinha et al.*, 2003]. The correlations of $\Delta M_{BC}/\Delta CO$, $\Delta M_{BC}/\Delta CO_2$, $\Delta V_{SC}/\Delta M_{BC}$, $\Delta M_{BC}/\Delta CH_3CN$, and $\Delta CH_3CN/\Delta CO$ versus MCE are shown in Figure 7. For this analysis, we have used all BB plume data, and slopes were estimated for different bins of MCE data. The emission ratios of $\Delta M_{BC}/\Delta CO$ and $\Delta CH_3CN/\Delta CO$ increased with the increase in MCE, while the emission ratios of $\Delta M_{BC}/\Delta CO_2$ and $\Delta V_{SC}/\Delta M_{BC}$ tended to decrease with the increase in MCE. During the ARCTAS-B period, the larger variability in the emission ratios were attributed to the sampling of BB plumes with a large range (0.6–0.99) of MCE. Similar to this study, the slopes of $\Delta M_{BC}/\Delta CO$ and $\Delta V_{SC}/\Delta CO$ increased with the increase in MCE, while $\Delta M_{BC}/\Delta CO_2$ and $\Delta V_{SC}/\Delta M_{BC}$ decreased with the increase in MCE. As described by *Sinha et al.* [2003], for many species the emission factors show negative correlation with MCE, indicating their preferential release during smoldering combustion. For some species emission factors are weakly correlated with MCE and do not strongly depend on the combustion process.

4. Microphysical Properties

4.1. Size Distributions of BC

[31] The average number and mass size distributions of BC observed in both FF and BB plumes are shown in Figures 8a and 8b. The size distribution presented in this section is for uncoated BC particles; however, the BC particles in ambient air are always coated. The count median diameter (CMD) and geometric standard deviation (σ_{gc}) were derived from a mono-modal lognormal distribution fit. The CMD and σ_{gc} calculated for each plume are presented in Table 5. In the FF type of plumes, the size distributions were very stable, with an average CMD of 115 ± 5 nm and σ_{gc} of 1.36. Similarly, the distributions were also unvarying, with a CMD of 141 ± 9 nm and σ_{gc} of 1.33 in BB plumes. The mass median diameter (MMD) and geometric standard deviation (σ_{gm}) were 175 ± 10 nm and 1.57 for FF plumes, while in the BB plumes they were 193 ± 16 nm and 1.46, respectively. Clearly, BC particles emitted from BB sources were populated in a large but narrower size range compared to FF plumes. In the BB plumes, the CMD and MMD of BC tended to decrease with increasing MCE. It is interesting to note that the size distribution parameters of BC in the mixed plume seem to represent the combined features of FF and BB distributions. The CMD = 129 (with σ_{gc} = 1.43) and MMD = 239 nm (σ_{gm} = 1.76) of BC in the mixed plume seem to characterize the convolution of size distributions of FF and BB plumes. In support to this statement, both σ_{gc} and σ_{gm} in mixed plume are larger compared to those estimated in both FF and BB plumes.

[32] The size distributions of BC in the BB plumes over California show good agreement with the mean CMD (136 ± 6 nm) and MMD (187 ± 10) nm observed in Canadian fire plumes during ARCTAS-B. *Kondo et al.* [2011b] have discussed the relationships of CMD and σ_{gc} with MCE in BB plumes. The observed anti-correlation between CMD and σ_{gc} of BC has been attributed to coagulation [*Kajino and Kondo*, 2011].

[33] Agreeing with the BC size distributions observed during the ARCTAS-B and ARCTAS-CARB phases, the MMDs were 170 nm and 210 nm in urban and BB plumes,

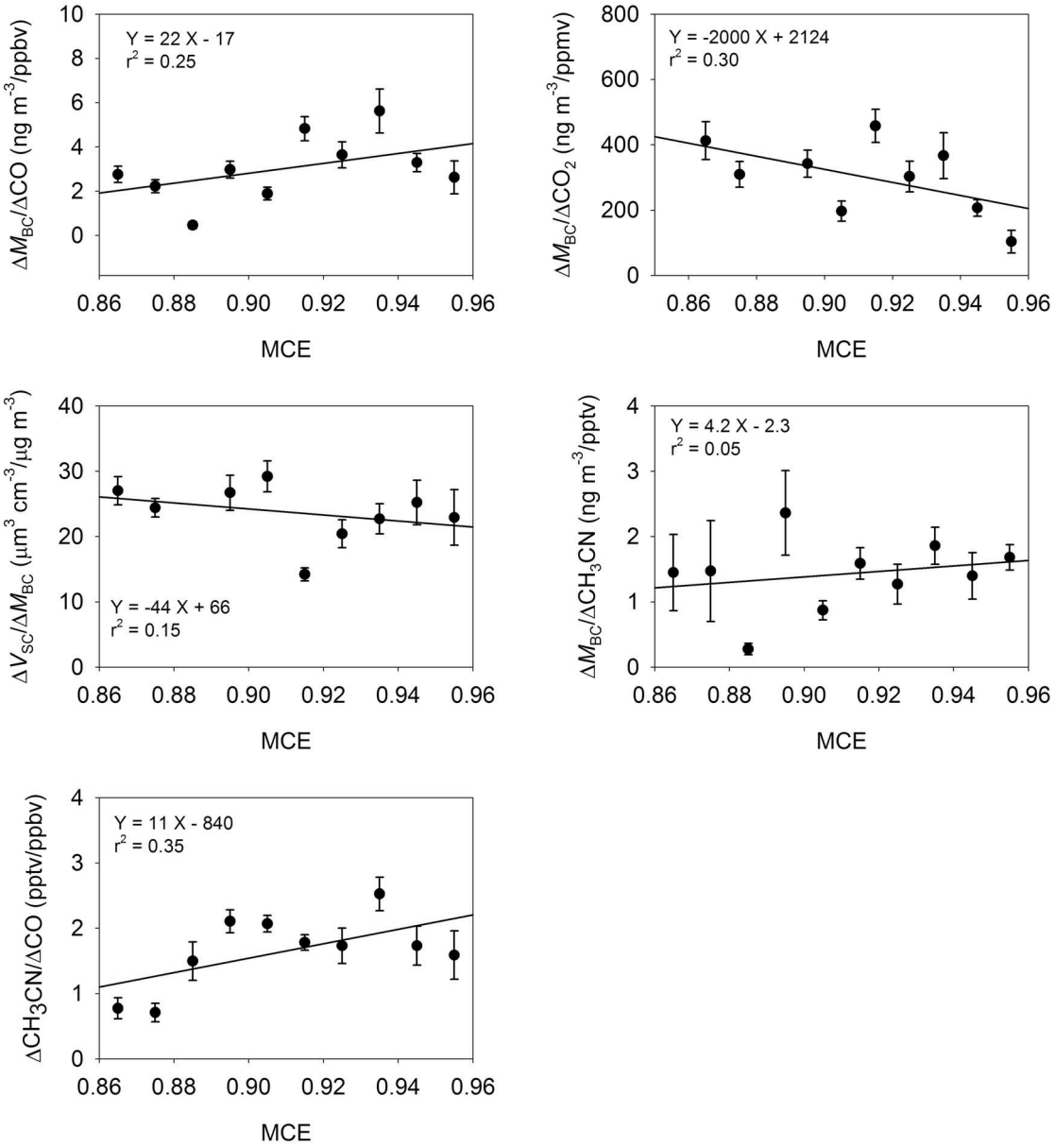

Figure 7. Scatterplots of $\Delta M_{BC}/\Delta CO$, $\Delta M_{BC}/\Delta CO_2$, $\Delta V_{SC}/\Delta M_{BC}$, $\Delta M_{BC}/\Delta CH_3CN$, and $\Delta CH_3CN/\Delta$ CO ratios versus MCE using BB plume data. Linear regression fits are also shown.

respectively, during the TexAQS campaign [*Schwarz et al.*, 2008]. The measurements of BC in urban plumes in Tokyo show a smaller MMD of 146 ± 12 nm, with a mean σ_{gm} of 1.82 ± 0.14 [*Kondo et al.*, 2011a]. In a slightly aged urban plume at the suburban site of Kisai in Tokyo, the MMD of BC were measured to be between 145 nm and 150 nm [*Shiraiwa et al.*, 2007]. Measurements of BC using an SP2 over western and northern Europe were made during the European integrated Project on Aerosol Cloud Climate and Air Quality Interactions – Long Range Experiment (EUCAARI-LONGREX), also referred as the LONGREX campaign [*McMeeking et al.*, 2010]. During this study, the BC particles measured in the fresh urban plumes showed lognormal distribution with a larger average MMD of 173 nm.

4.2. Size Distributions of LSP

[34] The average number and volume size distributions of LSP observed in both FF and BB plumes are shown in Figures 8c and 8d. The size distribution presented in this section is for LSP particles that do not contain a BC core. The size distributions of LSP were also well represented by a mono-modal lognormal function. The statistics of the number size distributions of LSP (CMD and σ_{gc}) for each plume are listed in Table 5. The average values of CMD were 206 ± 10 nm and 233 ± 19 nm in FF and BB plumes, respectively. The volume size distributions of LSP exhibited two distinct modes corresponding to FF and BB plumes. The averages of the volume median diameter (VMD) of LSP were 220 ± 35 nm and 290 ± 40 nm in FF and BB plumes,

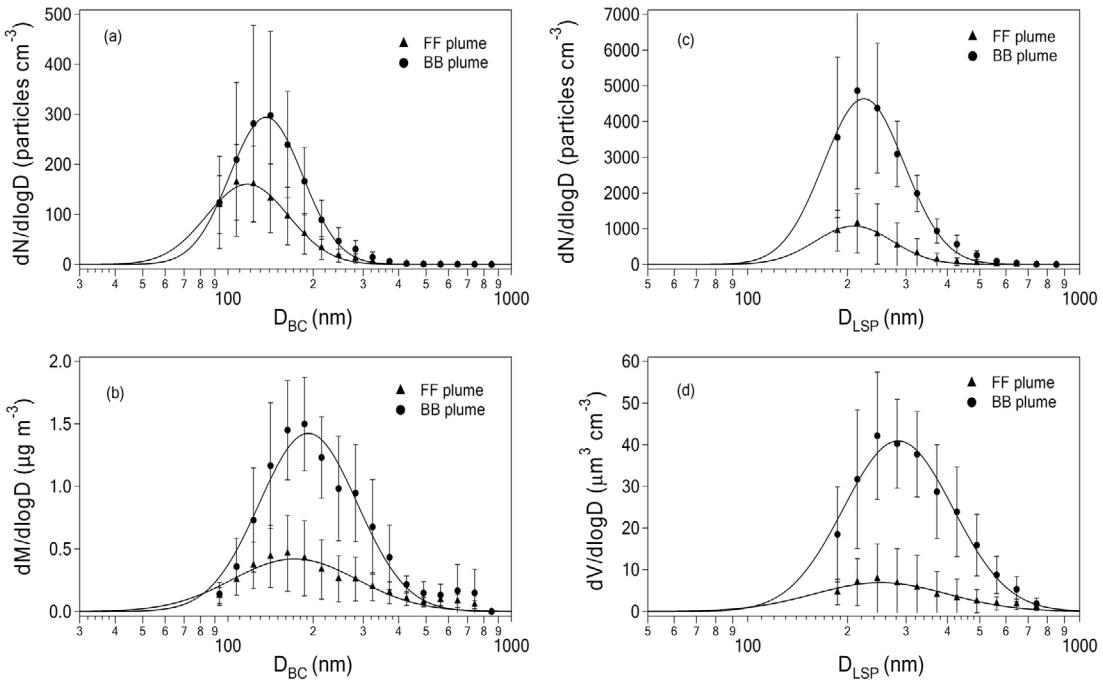

Figure 8. Mean size distributions of (a) BC number, (b) BC mass, (c) LSP number, and (d) LSP volume concentrations observed in FF and BB plumes over California during ARCTAS-CARB. Solid lines are mono-modal lognormal functions.

respectively. The geometric standard deviations (σ_{gv}) of the associated volume distribution were 1.66 and 1.41 in FF and BB plumes, respectively. In good agreement with the BB plumes of the present study, the CMD and VMD of LSP were estimated to be 224 ± 14 nm and 294 ± 42 nm, respectively, during ARCTAS-B. On the other hand, the larger CMD and VMD of 238 ± 11 nm and 306 ± 40 nm observed in the outflow from a Siberian fire during ARCTAS-A were attributed to the effects of both coagulation and condensation during transport. Measurements made at a remote island (Fukue, Japan) suggest a significantly larger MMD of 350–500 nm in different plumes in East Asian outflow [*Shiraiwa et al.*, 2008]. An understanding of the size distributions of aerosols requires detailed information of fuel type, fire intensity, combustion efficiency, and chemical composition. However, based on several field studies, the VMD of LSP emitted from forest fires show tight correlation with the emission factors of particles and unsaturated hydrocarbons [*Reid and Hobbs*, 1998]. The SP2 measurements do not provide the chemical signatures, so we have used AMS data for the chemical characterization of aerosols in FF and BB plumes. The sum of mass concentrations of non-refractory aerosols measured by AMS was tightly correlated with $V_{SC,}$ with $r^2 = 0.81$ during the ARCTAS-CARB campaign. The tight correlations between submicron dry particle volume determined by SP2 and speciated mass by AMS in both BB and FF plumes were also observed during the ARCPAC campaign [*Brock et al.*, 2011]. Therefore, we have used the AMS data to get

Table 5. Size Distributions of BC and LSP in the Different Plumes Observed During the ARCTAS-CARB Mission

	BC				LSP			
Plume Type	CMD (nm)	σ_{gc}	MMD (nm)	σ_{gm}	CMD (nm)	σ_{gc}	VMD (nm)	σ_{gv}
P1-FF	111	1.34	165	1.58	204	1.28	217	1.75
P2-FF	110	1.36	166	1.58	201	1.25	199	1.69
P3-FF	112	1.35	164	1.53	201	1.25	195	1.72
P4-BB	130	1.31	172	1.42	214	1.26	243	1.33
P5-FF	115	1.37	186	1.68	201	1.25	210	1.74
P6-BB	138	1.37	210	1.54	219	1.31	269	1.50
P7-FF	123	1.36	184	1.55	204	1.26	223	1.85
P8-Mix	129	1.43	239	1.76	227	1.35	307	1.58
P9-FF	121	1.40	182	1.52	226	1.32	281	1.43
P10-BB	144	1.35	195	1.44	246	1.36	321	1.40
P11-BB	150	1.30	195	1.41	253	1.35	325	1.39
Mean FF	115 ± 5	1.36 ± 0.02	175 ± 10	1.57 ± 0.06	206 ± 10	1.27 ± 0.02	220 ± 35	1.66 ± 0.13
Mean BB	141 ± 9	1.33 ± 0.03	193 ± 16	1.46 ± 0.06	233 ± 19	1.32 ± 0.04	290 ± 40	1.41 ± 0.07

Table 6. Average Mass Concentrations (μg STP m^{-3}) of BC, Inorganics, and Organic Aerosols in Different Plumes During ARCTAS-CARB

Plume Type	BC	Cl^-	NH_4^+	OA	NO_3^-	SO_4^{2-}	Sum
P1-FF	0.09	0.02	0.30	2.56	0.10	0.92	3.99
P2-FF	0.23	0.03	0.35	7.03	0.29	0.80	8.73
P3-FF	0.27	0.03	1.08	6.96	0.47	2.34	11.15
P4-BB	0.58	0.16	1.97	28.10	2.26	2.53	35.60
P5-FF	–	–	–	–	–	–	–
P6-BB	0.68	0.06	0.71	54.57	0.47	0.71	57.20
P7-FF	0.16	0.03	0.92	4.38	0.18	2.55	8.22
P8-Mix	0.50	0.07	0.47	3.16	0.23	1.17	5.60
P9-FF	0.51	0.04	0.68	9.76	0.69	1.01	12.69
P10-BB	0.45	0.04	0.45	11.17	0.36	0.63	13.10
P11-BB	0.28	0.07	0.98	13.78	0.61	2.40	18.12
Mean FF	0.25	0.03	0.67	6.14	0.35	1.52	8.96
SD FF	0.16	0.01	0.34	2.76	0.24	0.85	3.32
Mean BB	0.50	0.08	1.03	26.91	0.93	1.57	31.00
SD BB	0.17	0.05	0.66	19.89	0.90	1.04	19.95

information about different coating materials on BC cores in both FF and BB plumes.

4.3. Mixing State of BC Aerosol

[35] The mixing state of BC can be presented as shell/core diameter ratio (D_P/D_{BC}). In the present study, we have derived the shell/core ratio of BC for D_{BC} > 200 nm. We have studied the histograms of median shell/core ratios of BC in both FF and BB plumes using 10-s merged data. Apart from a few outliers, the D_P/D_{BC} in the FF and BB plumes varied within the ranges of 1.0–1.4 and 1.2–1.8, respectively. Overall, BC particles in the BB plume were thickly coated, with an average shell/core ratio of 1.47 compared to 1.24 in the FF plumes. By assuming spherical particle shapes, the volume fractions of coated BC particles (D_P^3/D_{BC}^3) were about 0.52 and 0.31 in FF and BB plumes, respectively. In other words, the mixing states of BC from the two source types in California differed significantly. Similarly, the distinct mixing states of BC in urban and BB plumes were also observed over Houston and Dallas during the TexAQS campaign [*Schwarz et al.*, 2008]. The average shell/core ratio of 1.48 estimated for Canadian forest fire plumes during ARCTAS-B shows excellent agreement with the present study. As discussed in section 5, the observed high shell/core ratio in BB compared to FF plumes is expected due to higher co-emissions of OA particles in BB plumes that will coagulate with the BC particles.

[36] The relationships of the mixing states of BC to the bulk and microphysical properties of aerosols have been demonstrated in previous studies [e.g., *McMeeking et al.*, 2011, and references therein]. We have investigated the relationships of the shell/core ratio with $\Delta V_{SC}/\Delta M_{BC}$ and VMD of LSP. In the FF plumes, the shell/core ratio does not show a clear dependence on $\Delta V_{SC}/\Delta M_{BC}$ or VMD but increases with the increase in both $V_{SC}/\Delta M_{BC}$ and VMD in the BB plumes. These relationships clearly demonstrate that the internal mixing states of BC particles depend on the emission ratio and size distributions of LSP. A simple model to assess the effect of coagulation between LSP and BC on the evolution of the BC mixing state has been discussed and applied to BB data measured during ARCTAS-B measurements [*Kajino and Kondo*, 2011; *Kondo et al.*, 2011b]. The reason we do not see such relationships in FF plumes could be due to the relatively lesser co-emissions of precursors of the coating materials. In moderately aged FF plumes, *Subramanian et al.* [2010] have reported a rather slower rate of BC coating over Mexico City. On the other hand, observations in East Asian outflow have shown that the coating thickness of BC-particles increased with time in sufficiently aged FF plumes [*Shiraiwa et al.*, 2008].

[37] Several studies have considered only condensation to explain the evolution of the mixing state of BC in FF plumes [*Moteki and Kondo*, 2007; *Shiraiwa et al.*, 2008]. In the BB plumes, the relationships of the shell/core ratio with $\Delta V_{SC}/\Delta M_{BC}$ and VMD of LSP support the suggestion that coagulation of LSP with BC can effectively increase the coating thickness [*Kondo et al.*, 2011b]. The dependence of the shell/core ratio on MCE and photochemical age has been discussed for BB plumes [*Kondo et al.*, 2011b]. The BC particles in BB plumes are rapidly coated due to enhanced co-emissions of coating materials [*Akagi et al.*, 2012]. In Canadian fire plumes, the volume of coating materials increased by ~40% within 12–24 h after emissions.

5. Chemical Characteristics of Aerosols

[38] The chemical composition of aerosols can provide information on the dominant sources and evolution of pollution in different plumes. *McNaughton et al.* [2011] have used a threshold value of 160 pptv of CH_3CN and an AMS organics (OA)/sulfate (SO_4^{2-}) ratio of >2.0 to separate BB-impacted air mass from that dominated by urban/industrial emissions. The average mass concentrations (in μg STP m^{-3}) of submicron non-refractory chemical components measured by the High-Resolution Time-of-Flight AMS (HR-ToF-AMS) [*DeCarlo et al.*, 2006; *Dunlea et al.*, 2009] for different plumes are presented in Table 6. The mass fractions of refractory and BC aerosols in each plume are presented in Table 7. The mass loading of measured submicron aerosols (sum of mass concentrations of OA, BC, ammonium (NH_4^+), nitrate (NO_3^-), SO_4^{2-}, and chloride (Cl^-)) of 31 μg m^{-3} in the BB plumes is significantly higher compared to 8.96 μg m^{-3} measured in the FF plumes. In both categories of sources, OA is the largest contributor, with averages of 6.14 ± 2.8 μg m^{-3} and 26.9 ± 19.9 μg m^{-3} in FF and BB plumes, respectively, followed by sulfate and nitrate aerosols. The average fractions of non-refractory and BC aerosols observed in FF and BB plumes are shown in Figure 9. The fractions of OA were 67.5% and 83.9% in FF and BB plumes, respectively. However, as expected, the SO_4^{2-} fraction of 18.44% in the FF plumes is large compared to 6.6% in the BB plumes. The sulfur (S) content in fossil fuels is higher compared to biomass vegetation [*Andreae and Merlet*, 2001; *Akagi et al.*, 2011]. Therefore, rather low SO_4^{2-} but high OA fractions are expected in the BB plumes, whereas in FF plumes sulfate is expected to be elevated. BC constituted smaller fractions of 2.6% in FF and 2.0% in BB plumes.

[39] In good agreement with the chemical compositions of BB plumes over California, similar fractions of OA (83%) and SO_4^{2-} (3–8%) were observed in Canadian fire plumes during ARCTAS-B. In the Siberian fire plumes over Alaska, however, influenced by long-range transport, a lesser amount of OA (60%) and higher SO_4^{2-} (30%) were observed during

Table 7. Average (±Standard Deviation) Mass Fractions (%) of BC, Inorganics, and Organic Aerosols in Different Plumes During ARCTAS-CARB

Plume Type	BC	Cl^-	NH_4^+	OA	NO_3^-	SO_4^{2-}
P1-FF	2.2 ± 1.7	0.5 ± 0.3	7.5 ± 3.7	64.2 ± 41.2	2.5 ± 2.0	23.1 ± 10.7
P2-FF	2.7 ± 1.1	0.3 ± 0.1	4.0 ± 0.8	80.5 ± 16.5	3.3 ± 1.2	9.2 ± 1.7
P3-FF	2.4 ± 1.0	0.3 ± 0.1	9.7 ± 5.0	62.4 ± 23.8	4.2 ± 3.8	21.0 ± 9.5
P4-BB	1.6 ± 0.9	0.4 ± 0.3	5.5 ± 2.7	78.9 ± 61.0	6.3 ± 4.5	7.1 ± 1.9
P5-FF	–	–	–	–	–	–
P6-BB	1.2 ± 0.5	0.1 ± 0.03	1.2 ± 0.4	95.4 ± 31.2	0.8 ± 0.3	1.2 ± 0.4
P7-FF	1.9 ± 1.0	0.4 ± 0.1	11.2 ± 6.1	53.3 ± 32.2	2.2 ± 2.0	31.0 ± 17.0
P8-Mix	8.9 ± 5.9	1.2 ± 1.1	8.4 ± 5.6	56.4 ± 24.2	4.1 ± 3.6	20.9 ± 14.5
P9-FF	4.0 ± 1.3	0.3 ± 0.1	5.4 ± 2.0	76.9 ± 7.9	5.4 ± 4.3	8.0 ± 1.9
P10-BB	3.5 ± 1.4	0.3 ± 0.1	3.4 ± 1.4	85.2 ± 39.3	2.7 ± 1.5	4.8 ± 1.4
P11-BB	1.5 ± 1.4	0.4 ± 0.2	5.4 ± 2.6	76.1 ± 40.1	3.4 ± 2.2	13.2 ± 11.5

the ARCTAS-A campaign [*Kondo et al.*, 2011b]. Similar to the aerosol loading in FF plumes over California, total AMS concentrations of 10–15 $\mu g\ m^{-3}$ were observed in urban plumes of London and northern England [*McMeeking et al.*, 2011]. However, the chemical compositions differed significantly, as the fractions of OA, (SO_4^{2-} + NH_4^+), and NO_3^-, were about 20%, 40%, and 40%, respectively, in the European FF plumes.

[40] To investigate the contribution to the coating on BC, the ratios of mass concentrations of non-refractory materials to BC can be applied by assuming that the coating composition matches the bulk aerosol composition [*Shiraiwa et al.*, 2008, and reference therein]. The relative amount of non-refractory materials with respect to BC has also been used to determine the net radiative forcing [*Ramana et al.*, 2010]. The individual ratios of OA/BC, SO_4^{2-}/BC, NH_4^+/BC, Cl^-/BC, and NO_3^-/BC observed in both types of plumes are presented in Table 8. The relative enhancements of OA and SO_4^{2-} aerosols were significantly higher than those in the other AMS species. The average OA/BC ratio of ~47 $\mu g\ \mu g^{-1}$ in the BB plumes was significantly higher compared to 26 $\mu g\ \mu g^{-1}$ observed in FF plumes. However, the SO_4^{2-}/BC ratio of 3.3 $\mu g\ \mu g^{-1}$ in the BB plumes was lower compared to 8.1 $\mu g\ \mu g^{-1}$ observed in the FF plumes. Significantly higher SO_4^{2-}/BC ratios for the Beijing, Shanghai, and "all-others" plumes were 16.6 $\mu g\ \mu g^{-1}$, 50 $\mu g\ \mu g^{-1}$, and 33 $\mu g\ \mu g^{-1}$, respectively, during the Cheju ABC Plume–Monsoon Experiment (CAPMEX) conducted in summer 2008 [*Ramana et al.*, 2010]. In the FF plumes, the average ratio of total non-refractory AMS to BC mass of 36 $\mu g\ \mu g^{-1}$ is significantly lower compared to 62 $\mu g\ \mu g^{-1}$ in the BB plumes.

[41] The ratio of NOx (=NO + NO_2) to total reactive nitrogen (NOy) has been used as an indicator of photochemical aging of air masses assuming NOy is emitted in the form of NOx [*Nunnermacker et al.*, 1998; *Kondo et al.*, 2008]. The NOx/NOy ratio decreases with increasing age of the air plume. We have examined the evolution of non-refractory aerosols by studying their dependencies on NOx/NOy. Figure 10 shows the BC-normalized mass concentrations of non-refractory aerosols and shell/core ratio as a function of NOx/NOy ratio in both FF and BB plumes. For most of the samples, the ratio of NOx/NOy in FF plumes was higher compared to those in BB plumes. This indicates that the FF plumes were systematically younger compared to the BB plumes. The mass ratios of non-refractory/BC tend to increase with the photochemical age, suggesting significant formation of secondary species in both types of plumes. However, the OA data are very scattered for the BB plumes, which is typical of the widely varying emission ratios of OA in BB plumes due to variations in fuel and combustion conditions [e.g., *Cubison et al.*, 2011] and it is not possible to estimate whether net SOA formation occurred in these particular plumes. Among the non-refractory species measured using AMS, the formation NO_3^- appears faster in the BB plumes compared to FF plumes. On the other hand, formation of SO_4^{2-} and NH_4^+ was faster in FF plumes compared to that in FF plumes. The increase in Cl^- with NOx/NOy implies the formation of secondary chloride, likely NH_4Cl, in the BB plumes. The higher $NH4^+$/BC ratio in the FF plumes indicates that these plumes were mixed with cattle-related sources from the CV. *Akagi et al.* [2012] have presented the evolution of non-refractory aerosols and trace gases emitted by a chaparral fire in California. The ratio of non-refractory/BC estimated after zero and 4.5 h since their emission have been used for comparison (see Table 8). The plume-averaged non-refractory/BC ratios estimated in this study are significantly higher compared to those measured in chaparral fire. The higher ratios of non-refractory/BC aerosols during ARCTAS-CARB could be due to the sampling of considerably aged air and smoldering phase products. Relatively higher ratios of SO_4^{2-} and Cl^- in BB plumes suggest the dominance of agricultural waste (crop residue) burning in the CV region [*Christian et al.*, 2010, and references therein].

6. Summary

[42] Airborne measurements of aerosols and trace gases were made over California during the NASA ARCTAS-CARB campaign, June 15–30, 2008. BC and LSP aerosols were measured by the SP2 technique on board the DC-8 aircraft. Emissions from the use of fossil fuels were the main source of aerosols and trace gases, while extensive forest fires were also reported over different parts of California during the campaign period. The major plumes originating from both anthropogenic (FF) and biomass burning (BB) sources were identified using CH_3CN and SO_2 (CH_2Cl_2) tracers, respectively. We have extracted the data to study the properties of BC and LSP in FF and BB plumes separately. In this paper, we have characterized the emission

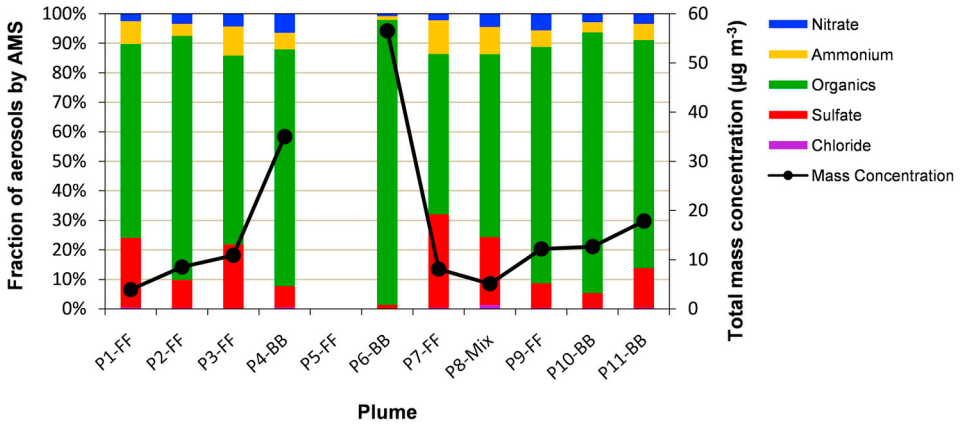

Figure 9. Fractions of major chemical components (AMS) and BC (SP2) in all FF and BB plumes identified over California during the ARCTAS-CARB 2008 campaign.

and microphysical properties of aerosols in the major plumes observed over different regions of California.

[43] The concentrations of both BC and LSP aerosols show large variations in both FF and BB plumes over California. In the BB plumes, the enhancements in the concentrations of aerosols and trace gases were significantly higher compared to those observed in the FF plumes. For example, the average mass concentrations of BC (M_{BC}) in FF and BB plumes were 243 ng m^{-3} and 513 ng m^{-3}, respectively. Overall, the aerosol loading was highest in the lower and middle troposphere, with very few particles observed in the upper troposphere. FF plumes were encountered mostly in the boundary layer, while the impacts of BB plumes were also observed in the middle troposphere.

[44] We have estimated the emission ratios of $\Delta CH_3CN/\Delta CO$, $\Delta CO/\Delta CO_2$, $\Delta V_{SC}/\Delta M_{BC}$, $\Delta M_{BC}/\Delta CO$, $\Delta M_{BC}/\Delta CO_2$, and $\Delta M_{BC}/\Delta CH_3CN$. Except for the $\Delta M_{BC}/\Delta CO$ ratio, distinct emission ratios of BC and LSP were observed in FF and BB plumes. The slope of $\Delta V_{SC}/\Delta M_{BC}$ is likely to be age dependent and may not represent the true emission ratio. The estimated emission ratios of $\Delta M_{BC}/\Delta CO$ were 3.16 ng m^{-3} $ppbv^{-1}$ and 3.28 ng m^{-3} $ppbv^{-1}$ in FF and BB plumes, respectively. In contrast to the $\Delta M_{BC}/\Delta CO$ ratio, the emission ratios of $\Delta M_{BC}/\Delta CO_2$ showed distinct values of 17.9 ng m^{-3} $ppmv^{-1}$ in FF plumes and 271.5 ng m^{-3} $ppmv^{-1}$ in BB plumes.

[45] Consistent with the classification of plumes, the average values of MCE were 0.898 and 0.995 for the BB and FF plumes, respectively. We have investigated the relationships between the emission ratio and MCE in the BB plumes. The emission ratios of $\Delta M_{BC}/\Delta CO$ and $\Delta CH_3CN/\Delta CO$ increased with the increase in MCE, while $\Delta M_{BC}/\Delta CO_2$ and $\Delta V_{SC}/\Delta M_{BC}$ tended to decrease with the increase in MCE. Overall, the emission ratios of BC in both plume types agreed reasonably well with previous values reported for North America. Most of the LSP did not contain BC, as the $\Delta V_{SC}/\Delta M_{BC}$ ratio of 23 cm^3 m^{-3}/g m^{-3} was about 4 times higher compared to those estimated in the FF plumes.

[46] The size distributions of both BC and LSP were well represented by a single-mode lognormal function. The size distributions of the number and mass concentrations of BC aerosols showed smaller CMD and MMD compared to those in BB plumes. The average CMDs of BC size distributions were 115 ± 5 nm (with σ_{gc} = 1.36) in FF plumes and 141 ± 9 nm (with σ_{gc} = 1.33) in BB plumes. Similarly, the LSP size distributions parameters (CMD, VMD, σ_{gc} and σ_{gv}) showed distinct values in the FF and BB plumes. The size distribution parameters of BC and LSP in the BB plumes showed very good agreement with those observed in the Canadian fire plumes during ARCTAS-B. The size distribution parameters of BC in the mixed plume seem to characterize the combined features of two distinct plumes, as σ_{gc} and σ_{gm} were larger compared to respective parameters in FF and BB plumes.

[47] The mixing state of BC was represented by the shell/core diameter ratio (D_P/D_{BC}). The BC particles in the BB plumes were thickly coated, as the mean D_P/D_{BC} of 1.47 was significantly larger compared to 1.24 in the FF plumes. The associated BC-core volume fractions of coated BC particles were estimated to be 0.52 and 0.31 in FF and BB plumes,

Table 8. Average Mass Concentration Ratios of Non-refractory and BC Aerosols Observed During ARCTAS-CARB and Comparison With Downwind Measurement of Chaparral Fire in California

	ARCTAS		Chaparral Fire	
Ratio	FF Plume (μg μg^{-1})	BB Plume (μg μg^{-1})	BB Plume (0 h)[a] (μg μg^{-1})	BB Plume (4.5 h)[a] (μg μg^{-1})
Ammonium/BC	3.2 ± 1.9	2.0 ± 1.4	0.077	0.0321
Nitrate/BC	1.3 ± 0.26	1.7 ± 1.5	0.12	0.53
OA/BC	26.3 ± 4.4	46.9 ± 23	4.53	3.88
Sulfate/BC	8.1 ± 5.7	3.3 ± 2.5	0.005	0.009
Chloride/BC	0.15 ± 0.06	0.18 ± 0.08	0.063	0.018

[a] *Akagi et al.* [2012].

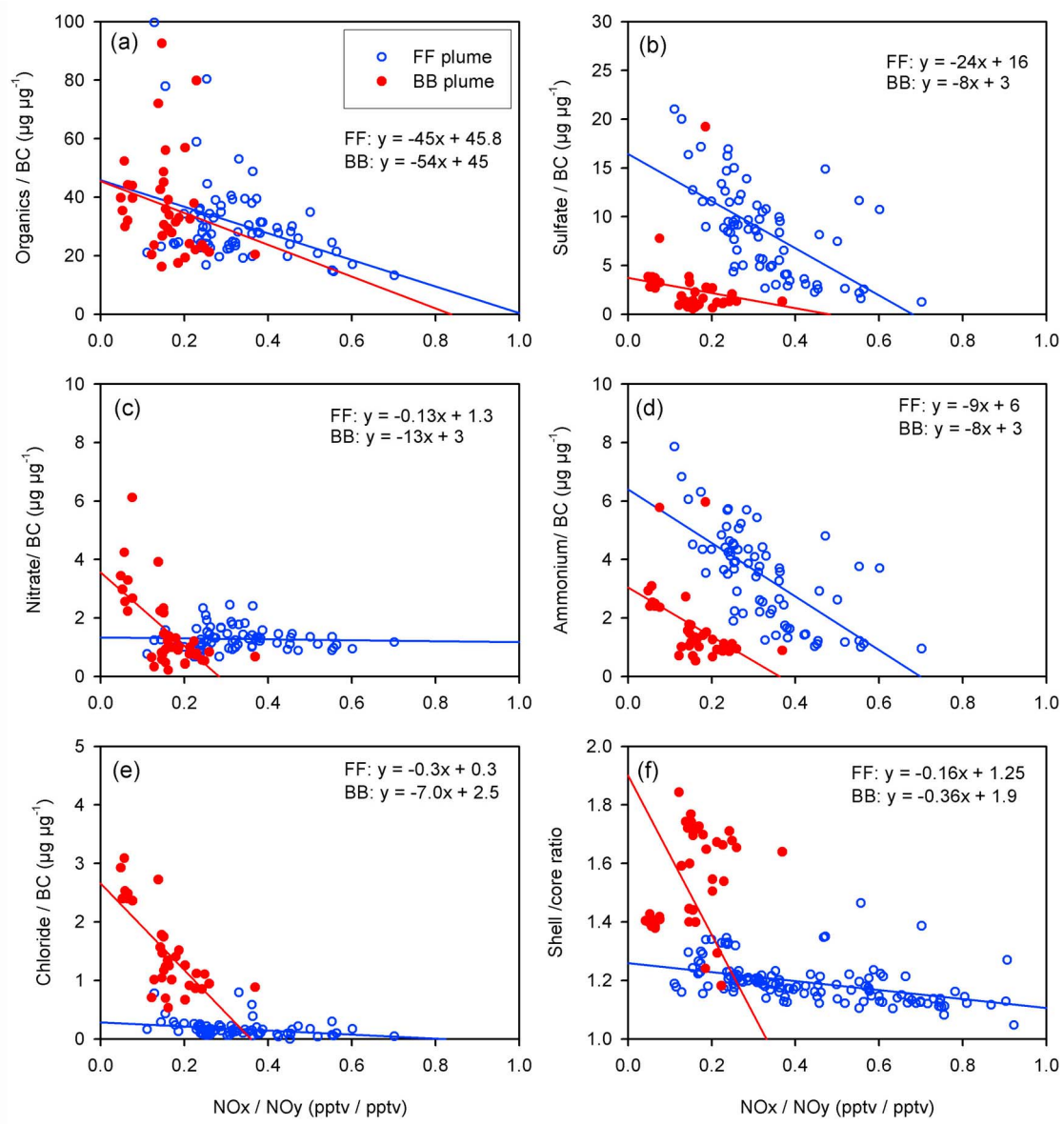

Figure 10. Scatterplots showing M_{BC}-normalized concentrations of non-refractory aerosols and shell/core ratio as a function of NOx/NOy ratio in both FF and BB plumes. Linear regression fits are also shown.

respectively. In the BB plumes, the D_P/D_{BC} ratio increased with the increase in both the $\Delta V_{SC}/\Delta M_{BC}$ emission ratio and VMD of LSP.

[48] In both categories of plumes, the mass concentration of OA was the largest contributor among other non-refractory aerosols. The mass fractions of OA were estimated to be about 67.5% and 84% in the FF and BB plumes, respectively. But the SO_4^{2-} aerosol mass fraction of 18.5% in FF plumes was higher compared to 6.6% observed in BB plumes. BC constituted smaller mass fractions of about 2.6% in the FF plumes and 2.0% in the BB plumes. In both FF and BB plumes, the ratios of non-refractory/BC aerosols increased with the decrease in NOx/NOy ratio due to photochemical aging. Overall, the ratios of non-refractory/BC aerosols in BB plumes during ARCTAS-CARB were significantly higher compared to a previous study reporting the evolution of aerosols in chaparral fire in California.

[49] **Acknowledgments.** The ARCTAS mission was supported by NASA. We are indebted to all the ARCTAS participants for their cooperation and support. Special thanks are due to the flight and ground crews of the NASA DC-8 aircraft. We thank M. Osuka for his assistance with the field measurements. P. O. Wennberg provided the SO_2 data used for the present study. This work was supported in part by the Ministry of Education, Culture, Sports, Science, and Technology (MEXT); the Strategic International Cooperative Program of the Japan Science and Technology Agency (JST); and the Global Environment Research Fund of the Japanese Ministry of the Environment (B-083). CH_3CN measurements were supported by the Austrian Research Promotion Agency (FFG-ALR) and the Tiroler Zukunftstiftung, operated with the help and support of M. Graus, A. Hansel, and T. D. Maerk. M. J. Cubison and J. L. Jimenez were supported by NASA NNX08AD39G and NNX12AC03G, CARB 08–319, and DOE (BER, ASR program) DE-SC0006035. Y. Zhao was supported in part by NASA's Tropospheric Chemistry Program (USP-SMD-08-009).

References

Ackerman, A. S., O. B. Toon, D. E. Stevens, A. J. Heymsfield, V. Ramanathan, and E. J. Welton (2000), Reduction of tropical cloudiness by soot, *Science*, *288*, 1042–1047, doi:10.1126/science.288.5468.1042.

Akagi, S. K., et al. (2011), Emission factors for open and domestic biomass burning for use in atmospheric models, *Atmos. Chem. Phys.*, *11*, 4039–4072, doi:10.5194/acp-11-4039-2011.

Akagi, S. K., et al. (2012), Evolution of trace gases and particles emitted by a chaparral fire in California, *Atmos. Chem. Phys.*, *12*(3), 1397–1421, doi:10.5194/acp-12-1397-2012.

Andreae, M. O., and P. Merlet (2001), Emission of trace gases and aerosols from biomass burning, *Global Biogeochem. Cycles*, *15*(4), 955–966, doi:10.1029/2000GB001382.

Arino, O., M. Simon, I. Piccolini, and J. M. Rosaz (2001), The ERS-2 ATSR-2 World Fire Atlas and the ERS-2 ATSR-2 World Burnt Surface Atlas projects, paper presented at 8th ISPRS Conference on Physical Measurement and Signatures in Remote Sensing, Eur. Space Agency, Aussois, France.

Bahadur, R., et al. (2011), Impact of California's air pollution laws on black carbon and their implications for direct radiative forcing, *Atmos. Environ.*, *45*(5), 1162–1167, doi:10.1016/j.atmosenv.2010.10.054.

Bauer, S. E., et al. (2010), A global modeling study on carbonaceous aerosol microphysical characteristics and radiative effects, *Atmos. Chem. Phys.*, *10*(15), 7439–7456, doi:10.5194/acp-10-7439-2010.

Baumgardner, D., G. Raga, O. Peralta, I. Rosas, T. Castro, T. Kuhlbusch, A. John, and A. Petzold (2002), Diagnosing black carbon trends in large urban areas using carbon monoxide measurements, *J. Geophys. Res.*, *107*(D21), 8342, doi:10.1029/2001JD000626.

Berner, A., S. Sidla, Z. Galambos, C. Kruisz, R. Hitzenberger, H. M. ten Brink, and G. P. A. Kos (1996), Modal character of atmospheric black carbon size distributions, *J. Geophys. Res.*, *101*(D14), 19,559–19,565, doi:10.1029/95JD03425.

Bohren, C. F., and D. R. Huffman (Eds.) (1998), *Absorption and Scattering of Light by Small Particles*, John Wiley, Hoboken, N. J., doi:10.1002/9783527618156

Bond, T. C., D. G. Streets, K. F. Yarber, S. M. Nelson, J.-H. Woo, and Z. Klimont (2004), A technology-based global inventory of black and organic carbon emissions from combustion, *J. Geophys. Res.*, *109*, D14203, doi:10.1029/2003JD003697.

Bond, T. C., G. Habib, and R. W. Bergstrom (2006), Limitations in the enhancement of visible light absorption due to mixing state, *J. Geophys. Res.*, *111*, D20211, doi:10.1029/2006JD007315.

Brock, C. A., et al. (2011), Characteristics, sources, and transport of aerosols measured in spring 2008 during the Aerosol, Radiation, and Cloud Processes Affecting Arctic Climate (ARCPAC) project, *Atmos. Chem. Phys.*, *11*, 2423–2453, doi:10.5194/acp-11-2423-2011.

Buongiorno, A., O. Arino, C. Zehner, P. Colagrande, and P. Goryl (1997), ERS-2 monitors exceptional fire event, *Earth Obs. Q.*, *56*, 1–6.

Chen, L.-W. A., B. G. Doddridge, R. R. Dickerson, J. C. Chow, P. K. Mueller, J. Quinn, and W. A. Butler (2001), Seasonal variations in elemental carbon aerosol, carbon monoxide and sulfur dioxide: Implications for sources, *Geophys. Res. Lett.*, *28*(9), 1711–1714, doi:10.1029/2000GL012354.

Christian, T. J., et al. (2010), Trace gas and particle emissions from domestic and industrial biofuel use and garbage burning in central Mexico, *Atmos. Chem. Phys.*, *10*(2), 565–584, doi:10.5194/acp-10-565-2010.

Cofer, W. R. I., J. S. Levine, E. L. Winstead, and B. J. Stocks (1991), Trace gas and particulate emissions from biomass burning in temperate ecosystems, in *Global Biomass Burning: Atmospheric, Climatic, and Biospheric Implication*, edited by J. S. Levine, pp. 203–208, MIT Press, Cambridge, Mass.

Conant, W. C., A. Nenes, and J. H. Seinfeld (2002), Black carbon radiative heating effects on cloud microphysics and implications for the aerosol indirect effect: 1. Extended Köhler theory, *J. Geophys. Res.*, *107*(D21), 4604, doi:10.1029/2002JD002094.

Cooke, W. F., and J. J. N. Wilson (1996), A global black carbon aerosol model, *J. Geophys. Res.*, *101*(D14), 19,395–19,409, doi:10.1029/96JD00671.

Cox, P., A. Delao, A. Komorniczak, and R. Weller (2009), The California almanac of emissions and air quality 2009 edition, report, 524 pp., Calif. Air Resour. Board, Sacramento, Calif. [Available at http://www. arb.ca.gov/aqd/almanac/almanac09/almanac2009all.pdf.]

Crounse, J., et al. (2006), Measurement of gas-phase hydroperoxides by chemical ionization mass spectrometry, *Anal. Chem.*, *78*, 6726–6732, doi:10.1021/ac0604235.

Crounse, J., et al. (2009), Biomass burning and urban air pollution over the Central Mexican Plateau, *Atmos. Chem. Phys.*, *9*, 4929–4944, doi:10.5194/acp-9-4929-2009.

Cubison, M. J., et al. (2011), Effects of aging on organic aerosol from open biomass burning smoke in aircraft and laboratory studies, *Atmos. Chem. Phys.*, *11*(23), 12,049–12,064, doi:10.5194/acp-11-12049-2011.

DeCarlo, P. F., et al. (2006), Field-deployable, high-resolution, time-of-flight aerosol mass spectrometer, *Anal. Chem.*, *78*, 8281–8289, doi:10.1021/ac061249n.

DeCarlo, P. F., et al. (2008), Fast airborne aerosol size and chemistry measurements above Mexico City and Central Mexico during the MILAGRO campaign, *Atmos. Chem. Phys.*, *8*, 4027–4048, doi:10.5194/acp-8-4027-2008.

de Gouw, J. A., C. Warneke, D. D. Parrish, J. S. Holloway, M. Trainer, and F. C. Fehsenfeld (2003), Emission sources and ocean uptake of acetonitrile (CH_3CN) in the atmosphere, *J. Geophys. Res.*, *108*(D11), 4329, doi:10.1029/2002JD002897.

de Gouw, J. A., et al. (2004), Chemical composition of air masses transported from Asia to the U.S. West Coast during ITCT 2K2: Fossil fuel combustion versus biomass-burning signatures, *J. Geophys. Res.*, *109*, D23S20, doi:10.1029/2003JD004202.

Delmas, R., J. P. Lacaux, and D. Brocard (1995), Determination of biomass burning emission factors: Method and results, *Environ. Monit. Assess.*, *38*, 181–204, doi:10.1007/BF00546762.

De Young, R. J., W. B. Grant, and K. Severance (2005), Aerosol transport in the California Central Valley observed by airborne lidar, *Environ. Sci. Technol.*, *39*, 8351–8357, doi:10.1021/es048740l.

Dunlea, E. J., et al. (2009), Evolution of Asian aerosols during transpacific transport in INTEX-B, *Atmos. Chem. Phys.*, *9*, 7257–7287, doi:10.5194/acp-9-7257-2009.

Fuelberg, H. E., D. L. Harrigan, and W. Sessions (2010), A meteorological overview of the ARCTAS 2008 mission, *Atmos. Chem. Phys.*, *10*, 817–842, doi:10.5194/acp-10-817-2010.

Gao, R. S., J. P. Schwarz, K. K. Kelly, D. W. Fahey, L. A. Watts, and T. L. Thompson (2007), A novel method for estimating light-scattering properties of soot aerosols using a modified single-particle soot photometer, *Aerosol Sci. Technol.*, *41*, 125–135, doi:10.1080/02786820601118398.

Guyon, P., et al. (2005), Airborne measurements of trace gas and aerosol particle emissions from biomass burning in Amazonia, *Atmos. Chem. Phys.*, *5*, 2989–3002, doi:10.5194/acp-5-2989-2005.

Hansen, A. D. A., T. J. Conway, L. P. Steele, B. A. Bodhaine, K. W. Thoning, P. Tans, and T. Novakov (1989), Correlations among combustion effluent species at Barrow, Alaska: Aerosol black carbon, carbon dioxide, and methane, *J. Atmos. Chem.*, *9*, 283–299, doi:10.1007/BF00052838.

Hansen, J., M. Sato, and R. Ruedy (1997), Radiative forcing and climate response, *J. Geophys. Res.*, *102*(D6), 6831–6864, doi:10.1029/96JD03436.

Hecobian, A., et al. (2011), Comparison of the chemical evolution and characteristics of 495 biomass burning plumes intercepted by the NASA DC-8 aircraft during the ARCTAS/CARB-2008 field campaign, *Atmos. Chem. Phys.*, *11*(24), 13,325–13,337, doi:10.5194/acp-11-13325-2011.

Hoff, R. M., S. P. Palm, J. A. Engel-Cox, and J. Spinhirne (2005), GLAS long-range transport observation of the 2003 California forest fire plumes to the northeastern US, *Geophys. Res. Lett.*, *32*, L22S08, doi:10.1029/2005GL023723.

Hornbrook, R. S., et al. (2011), Observations of nonmethane organic compounds during ARCTAS – Part 1: Biomass burning emissions and plume enhancements, *Atmos. Chem. Phys.*, *11*, 11,103–11,130, doi:10.5194/acp-11-11103-2011.

Huang, M., et al. (2011), Multi-scale modeling study of the source contributions to near-surface ozone and sulfur oxides levels over California during the ARCTAS-CARB period, *Atmos. Chem. Phys.*, *11*, 3173–3194, doi:10.5194/acp-11-3173-2011.

Intergovernmental Panel on Climate Change (IPCC) (2001), *Climate Change 2001: The Scientific Basis—Contribution of Working Group I to the Third Assessment Report of the Intergovernmental Panel on Climate Change*, edited by J. T. Houghton et al., Cambridge Univ. Press, New York.

Intergovernmental Panel on Climate Change (IPCC) (2007), *Climate Change 2007: The Physical Science Basis—Contribution of Working Group I to the Fourth Assessment Report of the Intergovernmental Panel on Climate Change*, edited by S. Solomon et al., Cambridge Univ. Press, New York.

Jacob, D. J., et al. (2010), The Arctic Research of the Composition of the Troposphere from Aircraft and Satellite (ARCTAS) mission: Design, execution, and first results, *Atmos. Chem. Phys.*, *10*, 5191–5212, doi:10.5194/acp-10-5191-2010.

Jacobson, M. Z. (2000), A physically based treatment of elemental carbon optics: Implications for global direct forcing of aerosols, *Geophys. Res. Lett.*, *27*, 217–220, doi:10.1029/1999GL010968.

Jacobson, M. Z. (2010), Short-term effects of controlling fossil-fuel soot, biofuel soot and gases, and methane on climate, Arctic ice, and air pollution health, *J. Geophys. Res.*, *115*, D14209, doi:10.1029/2009JD013795.

Janhäll, S., M. O. Andreae, and U. Pöschl (2010), Biomass burning aerosol emissions from vegetation fires: Particle number and mass emission factors and size distributions, *Atmos. Chem. Phys.*, *10*, 1427–1439, doi:10.5194/acp-10-1427-2010.

Kajino, M., and Y. Kondo (2011), EMTACS: Development and regional-scale simulation of a size, chemical, mixing type, and soot shape resolved atmospheric particle model, *J. Geophys. Res.*, *116*, D02303, doi:10.1029/2010JD015030.

Kim, S., et al. (2007), Measurement of pernitric acid in the free troposphere during the intercontinental chemical transport experiment–North America 2004, *J. Geophys. Res.*, *112*, D12S01, doi:10.1029/2006JD007676.

Koch, D., et al. (2009), Evaluation of black carbon estimations in global aerosol models, *Atmos. Chem. Phys.*, *9*, 9001–9026, doi:10.5194/acp-9-9001-2009.

Kondo, Y., et al. (2008), Formation and transport of oxidized reactive nitrogen, ozone, and secondary organic aerosol in Tokyo, *J. Geophys. Res.*, *113*, D21310, doi:10.1029/2008JD010134.

Kondo, Y., et al. (2009), Stabilization of the mass absorption cross section of black carbon for filter-based absorption photometry by the use of a heated inlet, *Aerosol Sci. Technol.*, *43*, 741–756, doi:10.1080/02786820902889879.

Kondo, Y., L. Sahu, N. Moteki, F. Khan, N. Takegawa, X. Liu, M. Koike, and T. Miyakawa (2011a), Consistency and traceability of black carbon measurements made by laser-induced incandescence, thermal-optical transmittance, and filter-based photo-absorption techniques, *Aerosol Sci. Technol.*, *45*, 295–312, doi:10.1080/02786826.2010.533215.

Kondo, Y., et al. (2011b), Emissions of black carbon, organic, and inorganic aerosols from biomass burning in North America and Asia in 2008, *J. Geophys. Res.*, *116*, D08204, doi:10.1029/2010JD015152.

Lesins, G., P. Chylek, and U. Lohmann (2002), A study of internal and external mixing scenarios and its effect on aerosol optical properties and direct radiative forcing, *J. Geophys. Res.*, *107*(D10), 4094, doi:10.1029/2001JD000973.

Li, Q., D. J. Jacob, I. Bey, R. M. Yantosca, Y. Zhao, Y. Kondo, and J. Notholt (2000), Atmospheric hydrogen cyanide (HCN): Biomass burning source, ocean sink?, *Geophys. Res. Lett.*, *27*(3), 357–360, doi:10.1029/1999GL010935.

Lighty, J. S., J. M. Veranth, and A. F. Sarofim (2000), Combustion aerosols: Factors governing their size and composition and implications to human health, *J. Air Waste Manage. Assoc.*, *50*, 1565–1618, doi:10.1080/10473289.2000.10464197.

Liousse, C., J. E. Penner, C. Chuang, J. J. Walton, H. Eddleman, and H. Cachier (1996), A global three-dimensional model study of carbonaceous aerosols, *J. Geophys. Res.*, *101*(D14), 19,411–19,432, doi:10.1029/95JD03426.

Matsui, H., et al. (2011), Seasonal variation of the transport of black carbon aerosol from the Asian continent to the Arctic during the ARCTAS aircraft campaign, *J. Geophys. Res.*, *116*, D05202, doi:10.1029/2010JD015067.

McMeeking, G. R., S. M. Kreidenweis, C. M. Carrico, T. Lee, J. L. Collett Jr., and W. C. Malm (2005), Observations of smoke-influenced aerosol during the Yosemite Aerosol Characterization Study: Size distributions and chemical composition, *J. Geophys. Res.*, *110*, D09206, doi:10.1029/2004JD005389.

McMeeking, G. R., et al. (2009), Emissions of trace gases and aerosols during the open combustion of biomass in the laboratory, *J. Geophys. Res.*, *114*, D19210, doi:10.1029/2009JD011836.

McMeeking, G. R., et al. (2010), Black carbon measurements in the boundary layer over western and northern Europe, *Atmos. Chem. Phys.*, *10*, 9393–9414, doi:10.5194/acp-10-9393-2010.

McMeeking, G. R., W. T. Morgan, M. Flynn, E. J. Highwood, K. Turnbull, J. Haywood, and H. Coe (2011), Black carbon aerosol mixing state, organic aerosols and aerosol optical properties over the United Kingdom, *Atmos. Chem. Phys.*, *11*, 9037–9052, doi:10.5194/acp-11-9037-2011.

McMurry, P. H., and X. Q. Zhang (1989), Size distribution of ambient organic and elemental carbon, *Aerosol Sci. Technol.*, *10*, 430–437, doi:10.1080/02786828908959282.

McNaughton, C. S., et al. (2011), Absorbing aerosol in the troposphere of the Western Arctic during the 2008 ARCTAS/ARCPAC airborne field campaigns, *Atmos. Chem. Phys.*, *11*, 7561–7582, doi:10.5194/acp-11-7561-2011.

Menon, S., J. E. Hansen, L. Nazarenko, and Y. Luo (2002), Climate effects of black carbon aerosols in China and India, *Science*, *297*, 2250–2253, doi:10.1126/science.1075159.

Miguel, A. H., T. W. Kirchstetter, R. A. Harley, and S. V. Hering (1998), On-road emissions of particulate polycyclic aromatic hydrocarbons and black carbon from gasoline and diesel vehicles, *Environ. Sci. Technol.*, *32*, 450–455, doi:10.1021/es970566w.

Mikhailov, E. F., S. S. Vlasenko, I. A. Podgorny, V. Ramanathan, and C. E. Corrigan (2006), Optical properties of soot–water drop agglomerates: An experimental study, *J. Geophys. Res.*, *111*, D07209, doi:10.1029/2005JD006389.

Moffet, R. C., and K. A. Prather (2009), In-situ measurements of the mixing state and optical properties of soot with implications for radiative forcing estimates, *Proc. Natl. Acad. Sci. U. S. A.*, *106*(29), 11,872–11,877, doi:10.1073/pnas.0900040106.

Moteki, N., and Y. Kondo (2007), Effects of mixing state on black carbon measurement by laser-induced incandescence, *Aerosol Sci. Technol.*, *41*, 398–417, doi:10.1080/02786820701199728.

Moteki, N., and Y. Kondo (2008), Method to measure time-dependent scattering cross sections of particles evaporating in a laser beam, *J. Aerosol Sci.*, *39*, 348–364, doi:10.1016/j.jaerosci.2007.12.002.

Moteki, N., and Y. Kondo (2010), Dependence of laser-induced incandescence on physical properties of black carbon aerosols: Measurements and theoretical interpretation, *Aerosol Sci. Technol.*, *44*, 663–675, doi:10.1080/02786826.2010.484450.

Nel, A. (2005), Air pollution-related illness: Effects of particles, *Science*, *308*(5723), 804–806, doi:10.1126/science.1108752.

Nenes, A., W. C. Conant, and J. H. Seinfeld (2002), Black carbon radiative heating effects on cloud microphysics and implications for the aerosol indirect effect: 2. Cloud microphysics, *J. Geophys. Res.*, *107*(D21), 4605, doi:10.1029/2002JD002101.

Nunnermacker, L. J., et al. (1998), Characterization of the Nashville urban plume on July 3 and July 18, 1995, *J. Geophys. Res.*, *103*(D21), 28,129–28,148, doi:10.1029/98JD01961.

Penner, J. E., H. Eddleman, and T. Novakov (1993), Towards the development of a global inventory for black carbon emissions, *Atmos. Environ., Part A*, *27*(8), 1277–1295.

Penner, J. E., C. C. Chuang, and K. Grant (1998), Climate forcing by carbonaceous and sulfate aerosols, *Clim. Dyn.*, *14*, 839–851, doi:10.1007/s003820050259.

Petters, M. D., C. M. Carrico, S. M. Kreidenweis, A. J. Prenni, P. J. DeMott, J. L. Collett Jr., and H. Moosmüller (2009), Cloud condensation nucleation activity of biomass burning aerosol, *J. Geophys. Res.*, *114*, D22205, doi:10.1029/2009JD012353.

Pfister, G. G., C. Wiedinmyer, and L. K. Emmons (2008), Impacts of the fall 2007 California wildfires on surface ozone: Integrating local observations with global model simulations, *Geophys. Res. Lett.*, *35*, L19814, doi:10.1029/2008GL034747.

Ramana, M. V., V. Ramanathan, Y. Feng, S.-C. Yoon, S.-W. Kim, G. R. Carmichael, and J. J. Schauer (2010), Warming influenced by the ratio of black carbon to sulphate and the black-carbon source, *Nat. Geosci.*, *3*, 542–545, doi:10.1038/ngeo918.

Ramanathan, V., et al. (2001), Indian Ocean Experiment: An integrated analysis of the climate forcing and effects of the great Indo-Asian haze, *J. Geophys. Res.*, *106*, 28,371–28,398, doi:10.1029/2001JD900133.

Ramanathan, V., et al. (2007), Atmospheric brown clouds: Hemispherical and regional variations in long-range transport, absorption, and radiative forcing, *J. Geophys. Res.*, *112*, D22S21, doi:10.1029/2006JD008124.

Reid, J. S., and P. V. Hobbs (1998), Physical and optical properties of young smoke from individual biomass fires in Brazil, *J. Geophys. Res.*, *103*(D24), 32,013–32,030, doi:10.1029/98JD00159.

Reid, J. S., R. Koppmann, T. F. Eck, and D. P. Eleuterio (2005), A review of biomass burning emissions part II: Intensive physical properties of biomass burning particles, *Atmos. Chem. Phys.*, *5*, 799–825, doi:10.5194/acp-5-799-2005.

Sachse, G. W., G. F. Hill, L. O. Wade, and M. G. Perry (1987), Fast-response, high precision carbon monoxide sensor using a tunable diode laser absorption technique, *J. Geophys. Res.*, *92*, 2071–2081, doi:10.1029/JD092iD02p02071.

Sahu, L. K., Y. Kondo, Y. Miyazaki, M. Kuwata, M. Koike, N. Takegawa, H. Tanimoto, H. Matsueda, S. C. Yoon, and Y. J. Kim (2009), Anthropogenic aerosols observed in Asian continental outflow at Jeju Island, Korea, in spring 2005, *J. Geophys. Res.*, *114*, D03301, doi:10.1029/2008JD010306.

Sahu, L. K., Y. Kondo, Y. Miyazaki, P. Pongkiatkul, and N. T. Kim Oanh (2011), Seasonal and diurnal variations of black carbon and organic carbon aerosols in Bangkok, *J. Geophys. Res.*, *116*, D15302, doi:10.1029/2010JD015563.

Sandvik, A., M. Biryulina, N. G. Kvamstø, J. J. Stamnes, and K. Stamnes (2007), Observed and simulated microphysical composition of arctic clouds: Data properties and model validation, *J. Geophys. Res.*, *112*, D05205, doi:10.1029/2006JD007351.

Schwarz, J. P., et al. (2006), Single-particle measurement of midlatitude black carbon and light-scattering aerosols from the boundary layer to

the lower stratosphere, *J. Geophys. Res.*, *111*, D16207, doi:10.1029/2006JD007076.

Schwarz, J. P., et al. (2008), Measurement of the mixing state, mass, and optical size of individual black carbon particles in urban and biomass burning emissions, *Geophys. Res. Lett.*, *35*, L13810, doi:10.1029/2008GL033968.

Shiraiwa, M., Y. Kondo, N. Moteki, N. Takegawa, Y. Miyazaki, and D. R. Blake (2007), Evolution of mixing state of black carbon in polluted air from Tokyo, *Geophys. Res. Lett.*, *34*, L16803, doi:10.1029/2007GL029819.

Shiraiwa, M., Y. Kondo, N. Moteki, N. Takegawa, L. K. Sahu, A. Takami, S. Hatakeyama, S. Yonemura, and D. R. Blake (2008), Radiative impact of mixing state of black carbon aerosol in Asian outflow, *J. Geophys. Res.*, *113*, D24210, doi:10.1029/2008JD010546.

Singh, H. B., et al. (2010), Pollution influences on atmospheric composition and chemistry at high northern latitudes: Boreal and California forest fire emissions, *Atmos. Environ.*, *44*, 4553–4564, doi:10.1016/j.atmosenv.2010.08.026.

Sinha, P., P. V. Hobbs, R. J. Yokelson, I. T. Bertschi, D. R. Blake, I. J. Simpson, S. Gao, T. W. Kirchstetter, and T. Novakov (2003), Emissions of trace gases and particles from savanna fires in southern Africa, *J. Geophys. Res.*, *108*(D13), 8487, doi:10.1029/2002JD002325.

Slowik, J. G., K. Stainken, P. Davidovits, L. R. Williams, J. T. Jayne, C. E. Kolb, D. R. Worsnop, Y. Rudich, P. DeCarlo, and J. L. Jimenez (2004), Particle morphology and density characterization by combined mobility and aerodynamic diameter measurements. Part 2: Application to combustion generated soot particles as a function of fuel equivalence ratio, *Aerosol Sci. Technol.*, *38*, 1206–1222, doi:10.1080/027868290903916.

Slusher, D. L., L. G. Huey, D. L. Tanner, F. M. Flocke, and J. M. Roberts (2004), A thermal dissociation-chemical ionization mass spectrometry (TD-CIMS) technique for the simultaneous measurement of peroxyacyl nitrates and dinitrogen pentoxide, *J. Geophys. Res.*, *109*, D19315, doi:10.1029/2004JD004670.

Spackman, J. R., J. P. Schwarz, R. S. Gao, L. A. Watts, D. S. Thomson, D. W. Fahey, J. S. Holloway, J. A. de Gouw, M. Trainer, and T. B. Ryerson (2008), Empirical correlations between black carbon aerosol and carbon monoxide in the lower and middle troposphere, *Geophys. Res. Lett.*, *35*, L19816, doi:10.1029/2008GL035237.

Stier, P., J. H. Seinfeld, S. Kinne, J. Feichter, and O. Boucher (2006), Impact of nonabsorbing anthropogenic aerosols on clear-sky atmospheric absorption, *J. Geophys. Res.*, *111*, D18201, doi:10.1029/2006JD007147.

Streets, D. G., et al. (2003), An inventory of gaseous and primary aerosol emissions in Asia in the year 2000, *J. Geophys. Res.*, *108*(D21), 8809, doi:10.1029/2002JD003093.

Subramanian, R., et al. (2010), Black carbon over Mexico: The effect of atmospheric transport on mixing state, mass absorption cross-section, and BC/CO ratios, *Atmos. Chem. Phys.*, *10*, 219–237, doi:10.5194/acp-10–219–2010.

Vay, S. A., et al. (2011), Patterns of CO_2 and radiocarbon across high northern latitudes during International Polar Year 2008, *J. Geophys. Res.*, *116*, D14301, doi:10.1029/2011JD015643.

Venkataraman, C., and S. K. Friedlander (1994), Size distribution of polycyclic aromatic hydrocarbons and elemental carbon. 2. Ambient measurements and effects of atmospheric processes, *Environ. Sci. Technol.*, *28*, 563–572, doi:10.1021/es00053a006.

Wang, Y., J. W. Munger, S. Xu, M. B. McElroy, J. Hao, C. P. Nielsen, and H. Ma (2010), CO_2 and its correlation with CO at a rural site near Beijing: Implications for combustion efficiency in China, *Atmos. Chem. Phys.*, *10*, 8881–8897, doi:10.5194/acp-10-8881-2010.

Ward, D. E., A. Setzer, Y. J. Kaufman, and R. A. Rasmussen (1991), Characteristics of smoke emissions from biomass fires of the Amazon region–Base-A experiment, in *Global Biomass Burning*, edited by J. S. Levine, pp. 394–402, MIT Press, Cambridge, Mass.

Ward, D., R. Susott, J. Kauffman, R. Babbitt, D. Cummings, B. Dias, B. Holben, Y. Kaufman, R. Rasmussen, and A. Setzer (1992), Smoke and fire characteristics for cerrado and deforestation burns in Brazil: BASE-B experiment, *J. Geophys. Res.*, *97*(D13), 14,601–14,619, doi:10.1029/92JD01218.

Warneke, C., et al. (2009), Biomass burning in Siberia and Kazakhstan as an important source for haze over the Alaskan Arctic in April 2008, *Geophys. Res. Lett.*, *36*, L02813, doi:10.1029/2008GL036194.

Weinheimer, A. J., J. G. Walega, B. A. Ridley, B. L. Gary, D. R. Blake, N. J. Blake, F. S. Rowland, G. W. Sachse, B. E. Anderson, and J. E. Collins (1994), Meridional distributions of NO_x, NO_y, and other species in the lower stratosphere and upper troposphere during AASE II, *Geophys. Res. Lett.*, *21*, 2583–2586, doi:10.1029/94GL01897.

Westerling, A. L., H. G. Hidalgo, D. R. Cayan, and T. W. Swetnam (2006), Warming and earlier spring increase western U. S. forest wildfire activity, *Science*, *313*(5789), 940–943, doi:10.1126/science.1128834.

Wisthaler, A., A. Hansel, R. R. Dickerson, and P. J. Crutzen (2002), Organic trace gas measurements by PTR-MS during INDOEX 1999, *J. Geophys. Res.*, *107*(D19), 8024, doi:10.1029/2001JD000576.

Wolff, G. T., P. J. Groblicki, S. H. Cadle, and R. J. Countess (1982), Particulate carbon at various locations in the United States, in *Particulate Carbon: Atmospheric Life Cycle*, edited by G. T. Wolff and R. L. Klimisch, pp. 297–315, Plenum Press, New York, doi:10.1007/978-1-4684-4154-3_17.

Yokelson, R. J., R. Susott, D. E. Ward, J. Reardon, and D. W. T. Griffith (1997), Emissions from smoldering combustion of biomass measured by open-path Fourier transform infrared spectroscopy, *J. Geophys. Res.*, *102*(D15), 18,865–18,877, doi:10.1029/97JD00852.

Yokelson, R. J., I. T. Bertschi, T. J. Christian, P. V. Hobbs, D. E. Ward, and W. M. Hao (2003), Trace gas measurements in nascent, aged, and cloud processed smoke from African savanna fires by airborne Fourier transform infrared spectroscopy (AFTIR), *J. Geophys. Res.*, *108*(D13), 8478, doi:10.1029/2002JD002322.

Yokelson, R. J., T. J. Christian, T. G. Karl, and A. Guenther (2008), The tropical forest and fire emissions experiment: Laboratory fire measurements and synthesis of campaign data, *Atmos. Chem. Phys.*, *8*, 3509–3527, doi:10.5194/acp-8-3509-2008.

Yokelson, R. J., et al. (2009), Emissions from biomass burning in the Yucatan, *Atmos. Chem. Phys.*, *9*(15), 5785–5812, doi:10.5194/acp-9-5785-2009.

Zuberi, B., K. S. Johnson, G. K. Aleks, L. T. Molina, and A. Laskin (2005), Hydrophilic properties of aged soot, *Geophys. Res. Lett.*, *32*, L01807, doi:10.1029/2004GL021496.